

Colloquium: Theory of Drag Reduction by Polymers in Wall Bounded Turbulence

Itamar Procaccia, Victor S. L'vov

Dept. of Chemical Physics, The Weizmann Institute of Science, Rehovot 76100, Israel

Roberto Benzi

Dip. di Fisica and INFN, Università "Tor Vergata", Via della Ricerca Scientifica 1, I-00133 Roma, Italy

The flow of fluids in channels, pipes or ducts, as in any other wall-bounded flow (like water along the hulls of ships or air on airplanes) is hindered by a drag, which increases many-folds when the fluid flow turns from laminar to turbulent. A major technological problem is how to reduce this drag in order to minimize the expense of transporting fluids like oil in pipelines, or to move ships in the ocean. It was discovered in the mid-twentieth century that minute concentrations of polymers can reduce the drag in turbulent flows by up to 80%. While experimental knowledge had accumulated over the years, the fundamental theory of drag reduction by polymers remained elusive for a long time, with arguments raging whether this is a "skin" or a "bulk" effect. In this colloquium review we first summarize the phenomenology of drag reduction by polymers, stressing both its universal and non-universal aspects, and then proceed to review a recent theory that provides a quantitative explanation of all the known phenomenology. We treat both flexible and rod-like polymers, explaining the existence of universal properties like the Maximum Drag Reduction (MDR) asymptote, as well as non-universal cross-over phenomena that depend on the Reynolds number, on the nature of the polymer and on its concentration. Finally we also discuss other agents for drag reduction with a stress on the important example of bubbles.

Contents

I. Introduction	1	C. Drag reduction in bubbly flows	20
A. Universality of Newtonian mean velocity profile	2	1. Drag reduction with rigid spheres	20
B. Drag reduction phenomenology	2	2. Drag reduction with flexible bubbles	21
1. The universal Maximum Drag Reduction asymptote	3	VIII. Summary and Discussion	21
2. Cross-overs with flexible polymers	3	Acknowledgments	22
3. Cross-overs with rod-like polymers	4	A. The Hidden Symmetry of the Balance Equations	22
II. Simple Theory of the von Kármán Law	5	References	23
III. The Universality of the MDR	6	I. INTRODUCTION	
A. Model equations for flows laden with flexible-polymers	6	The fact that minute concentrations of flexible polymers can reduce the drag in turbulent flows in straight tubes was first discovered by B.A. Toms and published in 1949 (Toms, 1949). This is an important phenomenon, utilized in a number of technological applications including the Trans-Alaska Pipeline System. By 1995 there were about 2500 papers on the subject, and by now there are many more. Earlier reviews include those by (de-Gennes, 1990; Hoyt, 1972; Landhal, 1973; Lumley, 1969; McComb, 1990; Sreenivasan and White, 2000; Virk, 1975), and others. In this introductory chapter we present some essential facts known about the phenomenon, to set up the theoretical discussions that will form the bulk of this review.	
B. Derivation of the MDR	8	It should be stated right away that the phenomenon of drag, which is distinguished from viscous dissipation, should be discussed in the context of wall-bounded flows. In homogeneous isotropic turbulence there exists <i>dissipation</i> (Lamb, 1879), which at every point of the flow equals $\nu_0 \nabla \mathbf{U}(\mathbf{r}, t) ^2$ where ν_0 is the kinematic viscosity and $\mathbf{U}(\mathbf{r}, t)$ is the velocity field as a function of position	
C. The universality of the MDR: theory	10		
IV. The "Additive Equivalence": the MDR of Rod-like Polymers	12		
A. Hydrodynamics with rod-like polymers	12		
B. The balance equations and the MDR	12		
V. Non-Universal Aspects of Drag Reduction: Flexible Polymers	13		
A. The efficiency of drag reduction for flexible polymers	13		
B. Drag reduction when polymers are degraded	14		
C. Other mechanism for cross-over	15		
VI. Cross-over Phenomena with Rod-like Polymers	16		
A. The attainment of the MDR as a function of concentration	16		
B. Cross-over phenomena as a function of the Reynolds number	16		
VII. Drag Reduction by Bubbles	17		
A. Average equations for bubbly flows: the additional stress tensor	18		
B. Balance equations in the turbulent boundary layer	19		
1. Momentum balance	19		
2. Energy balance	20		

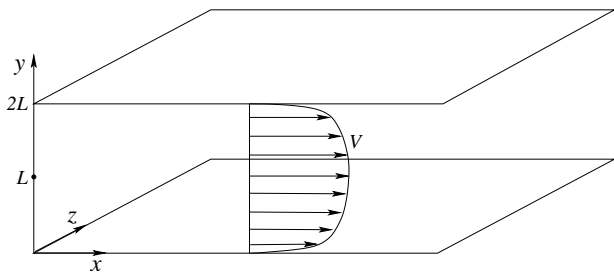


FIG. 1 The channel geometry

and time. The existence of a wall breaks homogeneity, and together with the boundary condition $\mathbf{U} = 0$ on the wall it sets a *momentum flux* from the bulk to the wall. This momentum flux is responsible for the drag, since not all the work done to push the fluid can translate into momentum in the stream-wise direction. In stationary condition all the momentum produced by the pressure head must flow to the wall. Understanding this (L'vov et al., 2004) is the first step in deciphering the riddle of the phenomenon of drag reduction by additives, polymers or others, since usually these agents tend to *increase the viscosity*. It appears therefore counter-intuitive that they would do any good, unless one understands that the main reason for drag-reduction when polymers or other drag-reducing agents are added to a Newtonian fluid is caused by reducing the momentum flux to the wall. The rest of this review elaborates on this point and makes it quantitative.

Contrary to the preference of the engineering community, in which arguments can rage about what is the *mechanism* of drag reduction, and whether these are hair-pin vortices or other ‘things’ that do the trick, we will adhere to the parlance of the physics community where a theory is tested by its quantitative predictiveness. We thus base our considerations on the analysis of model equations and their consequences. The criterion for validity will be our ability to describe and understand in a quantitative fashion all the observed phenomena of drag reduction, both universal and non-universal, and the ability to predict the results of yet unperformed experiments. The reader will judge for himself the extent of success of this approach.

A. Universality of Newtonian mean velocity profile

For concreteness we will focus on channel flows, but most of our observations will be equally applicable to other wall bounded flows. The channel geometry is sketched in Fig. 1. The mean flow is in the x direction, between two parallel plates displaced by a distance $2L$. The distance from the lower wall is denoted by y , and the span-wise direction by z . One takes the length of the channel in the x direction to be much larger than the distance between the side walls in z , and the latter much larger than L . In such a geometry the mean velocity

$V \equiv \langle \mathbf{U}(\mathbf{r}, t) \rangle$ is (to a high approximation) independent of either x or z , but only a function of the distance from the wall, $V = V(y)$. When a Newtonian fluid flows at large large Reynolds number (cf. Eq. (1.1) in such a channel, it exhibits in the near-wall region a *universal* mean velocity profile. Here we use the word “universal” in the sense that any Newtonian fluid flowing in the vicinity of a smooth surface will have the same mean velocity profile when plotted in the right coordinates. The universality is best displayed in dimensionless coordinates, known also as “wall units” (Pope, 2000); First, for incompressible fluids we can take the density as unity, $\rho = 1$. Then we define the Reynolds number \mathcal{Re} , the normalized distance from the wall y^+ and the normalized mean velocity $V^+(y^+)$ as follows:

$$\mathcal{Re} \equiv L\sqrt{p'L}/\nu_0, \quad y^+ \equiv y\mathcal{Re}/L, \quad V^+ \equiv V/\sqrt{p'L}. \quad (1.1)$$

Here p' is the fixed pressure gradient $p' \equiv -\partial p/\partial x$. The universal profile is shown in Fig. 2 with green circles [simulations of De-Angelis et al. (2003)] open circles (experiments) and a black continuous line [theory by L'vov et al. (2004)]. This profile has two distinct parts. For $y^+ \leq 6$ one observes the “viscous sub-layer” where

$$V^+(y^+) = y^+, \quad y^+ \leq 6 \quad (1.2)$$

(and see Subsect. 1.3 for a derivation), whereas for $y^+ \gtrsim 30$ one sees the celebrated universal von Kármán “log-law of the wall” which is written in wall units as

$$V^+(y^+) = \kappa_{\mathcal{K}}^{-1} \ln y^+ + B_{\mathcal{K}}, \quad \text{for } y^+ \gtrsim 30. \quad (1.3)$$

The law (1.3) is universal, independent of the nature of the Newtonian fluid; it had been a shortcoming of the theory of wall-bounded turbulence that the von Kármán constant $\kappa_{\mathcal{K}} \approx 0.436$ and the intercept $B_{\mathcal{K}} \approx 6.13$ had been only known from experiments and simulations (Monin and Yaglom, 1979; Zagarola and Smits, 1997). Some recent progress on this was made by Lo et al. (2005).

Having observed the universal profile for the mean velocity, it is easy to see that any theory that seeks to understand drag reduction by a change in viscosity (de-Gennes, 1990) is bound to fail, since the universal profile is written in reduced coordinates, and a change in the viscosity can result only in a re-parameterization of the profile. Indeed, drag reduction must mean a change in the universal profile, such that the velocity V^+ in reduced coordinates exceeds the velocity V^+ predicted by Eq. (1.3).

B. Drag reduction phenomenology

Here we detail some of the prominent features of drag reduction (Virk, 1975), all of which must be explained by a consistent theory. An immediate riddle that comes to mind is the following: the polymers are molecular in

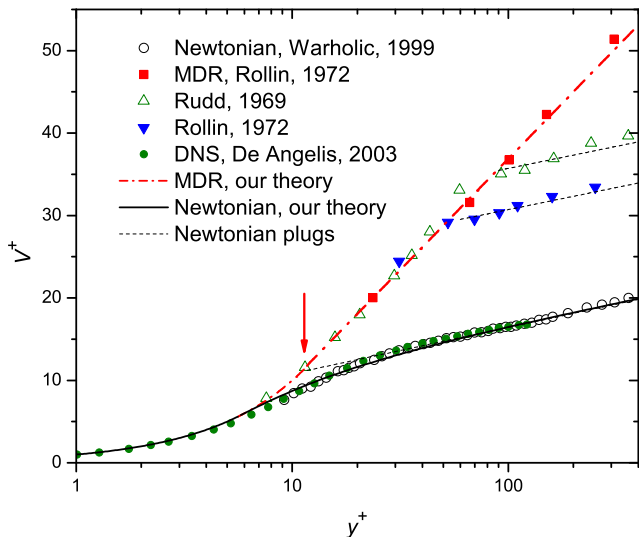


FIG. 2 Mean normalized velocity profiles as a function of the normalized distance from the wall. The data points (green circles) from numerical simulations of De-Angelis et al. (2003) and the experimental points (open circles (Warholic et al., 1999) refer to Newtonian flows. The solid line is a theoretical formula developed by L’vov et al. (2004). The red data points (squares) (Virk, 1975) represent the Maximum Drag Reduction (MDR) asymptote. The dashed red curve represents the log-law (1.5) which was derived from first principles by Benzi et al. (2005a). The blue filled triangles (Rollin, 1972) and green open triangles (Rudd, 1969) represent the cross-over, for intermediate concentrations of the polymer, from the MDR asymptote to the Newtonian plug.

scale. Turbulence is characterized by the outer scale L where energy is injected into the system, and by the Kolmogorov viscous scale η below which viscous dissipation dominates over inertial terms, and the velocity field becomes essentially smooth. For all realistic flows the polymer size is much smaller than this viscous scale (and cf. Subsec. III.A for some actual numbers for a typical polymer). How is it then that the polymers can interact at all with the turbulent degrees of freedom? This riddle was solve by Lumley (1969) who argued that it is the polymer relaxation time τ , the time that characterizes the relaxation of a stretched polymer back to its coiled equilibrium state, which is comparable to a typical eddy turn-over time in the turbulent cascade. This matching of time scales allows an efficient interaction between the turbulent fluctuations and the polymer degrees of freedom. With the typical shear rate $S(y)$ one forms a dimensionless “Deborah number”

$$\mathcal{De}(y) = \tau S(y) . \quad (1.4)$$

When \mathcal{De} exceeds the order of unity, the polymers begin to interact with the turbulent flow by *stretching* and taking energy from the turbulent fluctuations (cf. Subsec. III.A for a derivation of this). We will see below that this mechanism of Lumley is corroborated by all the available

data. What we will have to explain is how is it that as the polymers stretch, a process that must increase the viscosity, nevertheless the drag reduces.

1. The universal Maximum Drag Reduction asymptote

One of the most significant experimental findings (Virk, 1975) concerning turbulent drag reduction by polymers is that in wall-bounded turbulence (like channel and pipe flows) the velocity profile (with polymers added to the Newtonian fluid) is bounded between the von Kármán’s log-law (1.3) and another log-law which describes the maximal possible velocity profile (Maximum Drag Reduction, MDR),

$$V^+(y^+) = \kappa_v^{-1} \ln y^+ + B_v , \quad (1.5)$$

where $\kappa_v^{-1} \approx 11.7$ and $B_v \approx -17$. This law, which was discovered experimentally by Virk (1975) (and hence the notation κ_v), is also claimed to be universal, independent of the Newtonian fluid and the nature of the polymer additive, including flexible and rod-like polymers (Virk et al., 1997). This log-law, like von Kármán’s log-law, contains two phenomenological parameters. In (L’vov et al., 2004) it was shown that in fact this law contains only one parameter, and can be written in the form:

$$V^+(y^+) = \kappa_v^{-1} \ln (e \kappa_v y^+) \quad \text{for } y^+ \gtrsim 12 , \quad (1.6)$$

where e is the basis of the natural logarithm. The deep reason for this simplification will be explained below. For sufficiently high values of \mathcal{Re} , and sufficiently high concentration of the polymer c_p , and length of polymer (number of monomers N_p), the velocity profile in a channel is expected to follow the law (1.6). Needless to say, the first role of a theory of drag reduction is to provide an explanation for the MDR law and for its universality. We will explain below that the deep reason for the universality of the MDR is that it is a marginal state between a turbulent and a laminar regime of wall bounded-flows. In this marginal state turbulent fluctuations almost do not contribute to the momentum and energy balance, and the only role of turbulence is to extend the polymers in a proper way. This explanation can be found in Sect. III, including an a-priori calculation of the parameter κ_v . For finite \mathcal{Re} , finite concentration c_p , and finite number of monomers N_p , one expects cross-overs that are non-universal; in particular such cross-overs depend on the nature of the polymer, whether it is flexible or rod-like.

2. Cross-overs with flexible polymers

When the drag reducing agent is a flexible polymer, but the concentration c_p of the polymer is not sufficiently large, the mean velocity profiles exhibit a cross-over back to a log-law which is parallel to the law (1.3), but with a larger mean velocity (i.e. with a larger value of the intercept B_κ), see Fig. 2. The region of this log-law is known

as the “Newtonian plug”. The position of the cross-overs are not universal in the sense that they depend on the nature of the polymers and the flow conditions. The scenario is that the mean velocity profile follows the MDR up to a certain point after which it crosses back to the Newtonian plug. The layer of y^+ values between the viscous layer and the Newtonian plug is referred to as the “elastic layer”. A theory for these cross-overs is provided below. cf. Sect. V.

Another interesting experimental piece of information about cross-overs was provided by Choi et al. (2002). Here turbulence was produced in a counter-rotating disks apparatus, with λ -DNA molecules used to reduce the drag. The Reynolds number was relatively high (the results below pertain to $Re \approx 1.2 \times 10^6$) and the initial concentrations c_p of DNA were relatively low [results employed below pertain to $c_p = 2.70$ and $c_p = 1.35$ weight parts per million (wppm)]. During the experiment DNA degrades; fortunately the degradation is very predictable: double stranded molecules with 48 502 base pairs (bp) in size degrade to double stranded molecules with 23 100 bp. Thus invariably the length N_p reduces by a factor of approximately 2, and the concentration c_p increases by a factor of 2. The experiment followed the drag reduction efficacy measured in terms of the percentage drag reduction defined by

$$\%DR = \frac{T_N - T_V}{T_N} \times 100, \quad (1.7)$$

where T_N and T_V are the torques needed to maintain the disk to rotate at a particular Reynolds number without and with polymers, respectively. The main experimental results which are of interest to us are summarized in Fig. 3. We see from the experiment that both initially (with un-degraded DNA) and finally (with degraded DNA) the $\%DR$ is proportional to c_p . Upon degrading, which amounts to decreasing the length N_p by a factor of approximately 2 and, simultaneously increasing c_p by factor of 2, $\%DR$ decreases by a factor 4. Explanations of these findings can be found in Subsect. V.B.

3. Cross-overs with rod-like polymers

For the purposes of this review a flexible polymer is a polymer that is coiled at equilibrium or in a flow of low Reynolds number, and it undergoes a coil-stretch transition at some value of the Reynolds number, (see below for details). A rod-like polymer is stretched a-priori, having roughly the same linear extent at any value of the Reynolds number. When the polymers are rod-like and the concentration c_p is not sufficiently high, the cross-over scenario is different. The data in Fig. 4 include both flexible and rod-like polymers (Escudier et al., 1999). It again indicates that for large values of Re the mean velocity profile with flexible polymers [polyacrylamide (PAA)] follows the MDR until a point of cross-over back to the “Newtonian plug”, where it becomes

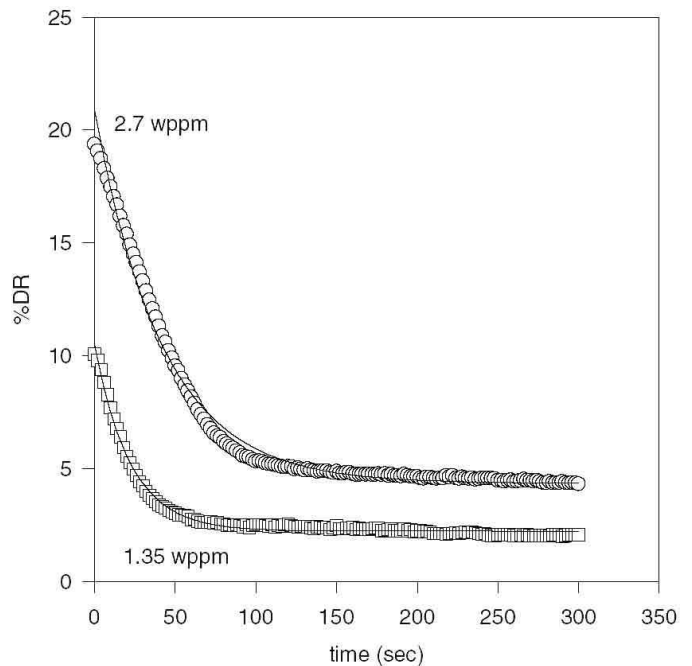


FIG. 3 $\%DR$ in a counter-rotating disks experiment with λ -DNA as the drag reducing polymer. Note that the $\%DR$ is proportional to c_p . When the length N_p reduces by a factor of 2 and, simultaneously, c_p increases by factor of 2, the $\%DR$ reduces by a factor of 4.

roughly parallel to von Kármán’s log-law. Increasing the concentration results in following the MDR further until a higher cross-over point is attained back to the Newtonian plug. On the other hand, for rod-like polymers [sodium carboxymethylcellulose (CMC) and sodium carboxymethylcellulose/xanthan gum blend (CMC/XG)] the data shown in Fig. 4 indicate a different scenario. Contrary to flexible polymers, here, as a function of the concentration, one finds mean velocity profiles that interpolate between the two asymptotes (1.3) and (1.5), reaching the MDR only for large concentrations. A similar difference in the behavior of flexible and rod-like polymers when plotting the drag as a function of Reynolds number was reported by Virk et al. (1997). Clearly, an explanation of these differences between the way the MDR is attained must be a part of the theory of drag reduction, and cf. Sect. VI. We reiterate that these cross-overs pertain to the situation in which Re is large, but c_p is too small.

Another major difference between the two classes of polymers is found when Re is too small, since then rod-like polymers can cause drag *enhancement*, whereas flexible polymer never cause drag enhancement. The latter are either neutral or cause drag reduction. The best way to see the phenomenon of drag enhancement at low Re with rod-like polymers is to consider the Fanning drag coefficient defined as

$$f \equiv \tau_* / \left(\frac{1}{2} \rho \tilde{V}^2 \right), \quad (1.8)$$

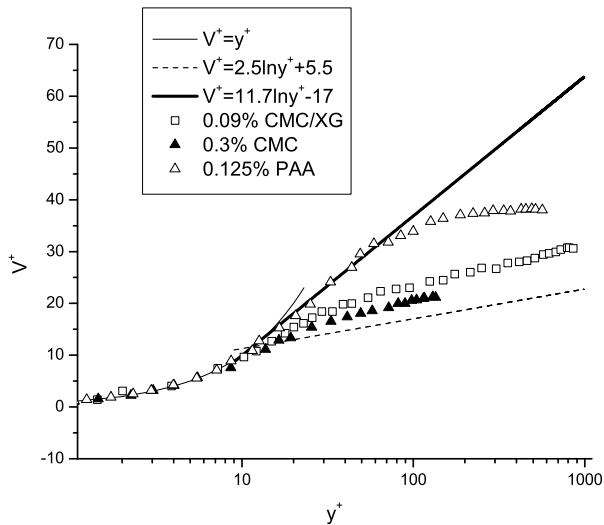


FIG. 4 Typical velocity profiles taken from (Escudier et al., 1999). In dashed line we noted the von Kármán law (1.3), while the MDR (1.6) is shown as the continuous black line. In all cases the mean velocity follows the same viscous behavior for $y^+ < 10$. After that the scenario is different for flexible and rod-like polymers. The typical behavior for the former is presented by the open triangles, which follow the MDR up to a cross-over point that depends on the concentration of the polymer and on the value of Re . The rod-like behavior is exemplified by the solid triangles and the open squares; the mean velocity profiles appear to interpolate smoothly between the two asymptotes as a function of the concentration of the rod-like polymer.

where τ_* is the shear stress at the wall, determined by the value $S(y=0)$ of the shear at $y=0$:

$$\tau_* \equiv \rho \nu_0 S(y=0), \quad (1.9)$$

ρ and \tilde{V} are the fluid density and the mean fluid throughput, respectively. Fig. 5 presents this quantity as a function of Re in the traditional Prandtl-Karman coordinates $1/\sqrt{f}$ vs. $Re\sqrt{f}$, for which once again the Newtonian high Re log-law is universal, and for which also there exists and MDR universal maximum (Virk, 1975; Virk et al., 1996). The straight continuous line denoted by ‘N’ presents the Newtonian universal law. Data points below this line are indicative of a drag enhancement, i.e., an increase in the dissipation due to the addition of the polymer. Conversely, data points above the line correspond to drag reduction, which is always bound by the MDR asymptote represented by the dashed line denoted by ‘M’. This figure shows data for a rod-like polymer (a polyelectrolyte in aqueous solution at very low salt concentration) and shows how drag enhancement for low values of Re crosses over to drag reduction at large values of Re (Virk et al., 1996; Wagner et al., 2003). One of the results of the theory presented below is that it reproduces the phenomena shown in Fig. 5 in a satisfactory manner.

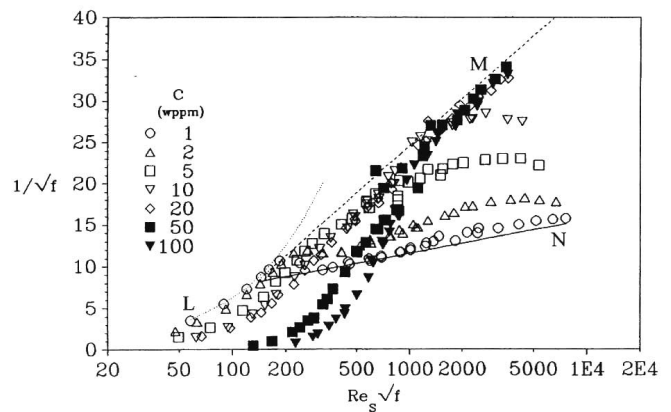


FIG. 5 The drag in Prandtl-Kármán coordinates for a low concentration solution of NaCl in water mixed with the rod-like polymer PAMH B1120 in a pipe flow, see (Virk et al., 1996) for details. The symbols represent the concentrations in wppm (weight parts per million) as given in the figure.

We reiterate that with *flexible* polymers the situation is very different, and there is no drag enhancement at any value of Re . The reason for this distinction will be made clear below as well.

II. SIMPLE THEORY OF THE VON KÁRMÁN LAW

As an introduction to the derivation of the MDR asymptote for fluids laden with polymers we remind the reader first how the von Kármán log-law (1.3) is derived. The derivation of the MDR will follow closely similar ideas with the modifications due to the polymers taken carefully into account.

Wall-bounded turbulence in Newtonian fluids is discussed (Monin and Yaglom, 1979; Pope, 2000) by considering the fluid velocity $\mathbf{U}(\mathbf{r})$ as a sum of its average (over time) and a fluctuating part:

$$\mathbf{U}(\mathbf{r}, t) = V(y)\hat{x} + \mathbf{u}(\mathbf{r}, t). \quad (2.1)$$

The objects that enter the Newtonian theory are the mean shear $S(y)$, the Reynolds stress $W(y)$ and the kinetic energy density per unit mass $K(y)$:

$$S(y) \equiv dV(y)/dy, \quad W(y) \equiv -\langle u_x u_y \rangle, \quad K(y) = \langle |\mathbf{u}|^2 \rangle / 2. \quad (2.2)$$

Note that the Reynolds stress is nothing but the momentum in the stream-wise direction x transported by the fluctuations u_y in the direction of the wall; it is the momentum flux to the wall. Using the Navier-Stokes equations one can calculate this momentum flux $P(y)$ which is generated by the pressure head $p' = -\partial p / \partial x$; at a distance y from the wall this flux is (Pope, 2000)

$$P(y) = p'(L - y). \quad (2.3)$$

We will be interested in positions $y \ll L$, so that we can approximate the production of momentum by a constant

$p'L$. This momentum is then dissipated at a rate $\nu_0 S(y)$. This give rise to the *exact* momentum balance equation

$$\nu_0 S(y) + W(y) = p'L, \quad y \ll L. \quad (2.4)$$

The two terms on the LHS take their main roles at different values of y . For y close to the wall the viscous term dominates, predicting that $S(y) \approx p'L/\nu_0$. This translates immediately to Eq. (1.2), the mean velocity profile close to the wall.

Away from the wall the Reynolds stress dominates, but all that can be learned is that $W(y) \approx \text{constant}$, which is not enough to predict the velocity profile. We need now to invoke a second equation that describes the energy balance.

Directly from the Navier-Stokes equations one can compute the rate of turbulent kinetic energy production by the mean shear, it is $W(y)S(y)$ (see for example Pope (2000)), and the energy dissipation E_d at any point, $E_d = \nu_0(|\nabla \mathbf{u}(\mathbf{r}, t)|^2)$. The energy dissipation is estimated differently near the wall and in the bulk (L'vov et al., 2004). Near the wall the velocity is smooth and we can estimate the gradient by the distance from the wall, and thus $E_d \approx \nu_0 a^2 K(y)/y^2$ where a is a dimensionless coefficient of the order of unity. Further away from the wall the flow is turbulent, and we estimate the energy flux by $K(y)/\tau(y)$ where $\tau(y) \approx y/b\sqrt{K(y)}$ is the typical eddy turn-over time at a distance y from the wall, and b is another dimensionless coefficient of the order of unity. Putting things together yields the energy balance equation

$$\left[\nu_0 \frac{a^2}{y^2} + \frac{b\sqrt{K}}{y} \right] K(y) = W(y)S(y), \quad (2.5)$$

where the first term is dominant near the wall and the second in the bulk. The interpretation of this equation is similar to the momentum balance equation except that the latter is exact; the first term on the LHS is the viscous dissipation, the second the energy flux to the wall, and the RHS is the production.

To close the problem, the balance equations need to be supplemented by a relation between $K(y)$ and $W(y)$. Dimensionally these objects are the same, and therefore in the bulk [where one uses dimensional analysis to derive the second term of (2.5)], we expect that these objects must be proportional to each other. Indeed, experiments and simulations (Ptasinski et al., 2001; Virk, 1975) corroborate this expectation and one writes (L'vov et al., 2004, 2005c)

$$W(y) = c_N^2 K(y), \quad (2.6)$$

with c_N being apparently y -independent outside the viscous boundary layer. To derive the von Kármán log-law we now assert that in the bulk the first term on the LHS of (2.5) is negligible, we then use Eq. (2.6) together with the previous conclusion that $W(y) = \text{const.}$ to derive immediately $S(y) \propto 1/y$. Integrating yields the von

Kármán log-law. Note that on the face of it we have three phenomenological parameters i.e. a , b and c_N . In fact in the calculation of the mean velocity they appear in two combination which can be chosen as κ_κ and B_κ in Eq. (1.3). Nevertheless it is not known how to compute these two parameters a-priori. Significantly, we will argue below that the slope of the MDR can be computed a-priori, cf. Subsect. III.C.

III. THE UNIVERSALITY OF THE MDR

To study the implications of adding small concentrations of polymers into wall-bounded turbulent flows we need a model that describes reliably the modifications in the hydrodynamic equations that are induced by the polymers. In the present section we are aiming at the universal, model independent properties of drag reduction, and therefore any reasonable model of polymers interacting with hydrodynamics which exhibits drag reduction should also lead to the universal properties. We begin with the case of flexible polymers.

A. Model equations for flows laden with flexible-polymers

To give a flavor of the type of polymers most commonly used in experiments and technological applications of drag reduction we present the properties of Polyethylene oxide ($N \times [-\text{CH}_2-\text{CH}_2-\text{O}]$, known as PEO). The typical number N of monomers ranges between 10^4 and 10^5 . In water solution in equilibrium this polymer is in a coiled state, with an end-to-end distance ρ_0 of about 10^{-7} m. When fully stretched the maximal end-to-end distance ρ_m is about 5×10^{-6} m. The typical mass concentration used is between 10 to 1000 wppm. The viscosity of the water solution increases by a factor of 2 when PEO is added with concentration of 280 wppm. Note that even the maximal value value ρ_m is much smaller than the typical Kolmogorov viscous scale, allowing us to model the turbulent velocity around such a polymer as a fluctuating homogeneous shear.

Although the polymer includes many monomers and therefore many degrees of freedom, it was shown during years of research (Beris and Edwards, 1994; Bird et al, 1987; de-Gennes, 1979; Flory, 1953) that the most important degree of freedom is the end-to-end distance, allowing the simplest model of the polymer to be a dumbbell of two spheres of radius \tilde{a} and negligible mass, connected by a spring of equilibrium length ρ_0 , characterized by a spring constant k . This model allows an easy understanding of the coil-stretch transition under a turbulent shear flow. If such a dumbbell is stretched to length ρ_p , the restoring force $k(\rho_p - \rho_0)$ is balanced by the Stokes force $6\pi\tilde{a}\nu_0 d\rho_p/dt$ (recall that the fluid density was taken as unity). Thus the relaxation time τ of the dumbbell is $\tau = 6\pi\tilde{a}\nu_0/k$. On the other hand, in the presence of a homogeneous shear S , the spring is stretched by a Stokes

force $6\pi\tilde{a}\nu_0 S\rho_p$. Balancing the stretching force with the restoring force (both proportional to ρ_p for $\rho_p \gg \rho_0$), one finds that the coil-stretch transition is expected when $S\tau > 1$. In fact, a free polymer will rotate under a homogeneous shear, making this argument a bit more involved. Indeed, one needs a *fluctuating* shear s in order to stretch the polymer, leading finally to the condition

$$\mathcal{De} \approx \tau \sqrt{\langle s^2 \rangle} > 1. \quad (3.1)$$

To obtain a consistent hydrodynamic description of polymer laden flows one needs to consider a field of polymers instead of a single chain. In a turbulent flow one can assume that the concentration of the polymers is well mixed, and approximately homogeneous. Each chain still has many degrees of freedom. However, as a consequence of the fact that the most important degree of freedom for a single chain is the end-to-end distance, the effects of the ensemble of polymers enters the hydrodynamics in the form of a ‘‘conformation tensor’’ $R_{ij}(r, t)$ which stems from the ensemble average of the dyadic product of the end-to-end distance of the polymer chains (Beris and Edwards, 1994; Bird et al, 1987), $R_{\alpha\beta} \equiv \langle \rho_\alpha \rho_\beta \rangle$. A successful model that had been employed frequently in numerical simulations of turbulent channel flows is the so-called FENE-P model (Bird et al, 1987), which takes into account the finite extensibility of the polymers:

$$\frac{\partial R_{\alpha\beta}}{\partial t} + (U_\gamma \nabla_\gamma) R_{\alpha\beta} = \frac{\partial U_\alpha}{\partial r_\gamma} R_{\gamma\beta} + R_{\alpha\gamma} \frac{\partial U_\beta}{\partial r_\gamma} - \frac{1}{\tau} [P(r, t) R_{\alpha\beta} - \rho_0^2 \delta_{\alpha\beta}], \quad (3.2)$$

$$P(r, t) = (\rho_m^2 - \rho_0^2) / (\rho_m^2 - R_{\gamma\gamma}). \quad (3.3)$$

The finite extensibility is reflected by the Peterlin function $P(r, t)$ which can be understood as a ensemble averaging correction to the potential energy $k(\rho - \rho_0)^2/2$ of the individual springs. For hydrodynamicists this equation should be evident: think about magneto-hydrodynamics, and the equations for the magnetic field \mathbf{n} . Write down the equations for the diadic product $n_\alpha n_\beta$; the inertial terms will be precisely the first line of Eq. (3.2). Of course, the dynamo effect would then tend to increase the magnetic field, potentially without limit; the role of the second line in the equation is to guarantee that the finite polymer will not stretch without limit, and the Peterlin term guarantees that when the polymer stretches close to the maximum there will be rapid exponential decay back to equilibrium values of the trace of \mathbf{R} . Since in most applications $\rho_m \gg \rho_0$ the Peterlin function can also be written approximately as $P(r, t) \approx 1/(1 - \gamma R_{\gamma\gamma})$ where $\gamma = \rho_m^{-2}$. In its turn the conformation tensor appears in the equations for fluid velocity $U_\alpha(r, t)$ as an additional stress tensor:

$$\frac{\partial U_\alpha}{\partial t} + (U_\gamma \nabla_\gamma) U_\alpha = -\nabla_\alpha p + \nu_0 \nabla^2 U_\alpha + \nabla_\gamma T_{\alpha\gamma}, \quad (3.4)$$

$$T_{\alpha\beta}(r, t) = \frac{\nu_p}{\tau} \left[\frac{P(r, t)}{\rho_0^2} R_{\alpha\beta}(r, t) - \delta_{\alpha\beta} \right]. \quad (3.5)$$

Here ν_p is a viscosity parameter which is related to the concentration of the polymer, i.e. $\nu_p/\nu_0 \sim c_p$ where c_p is the volume fraction of the polymer. We note however that the tensor field can be rescaled to get rid of the parameter γ in the Peterlin function, $\tilde{R}_{\alpha\beta} = \gamma R_{\alpha\beta}$ with the only consequence of rescaling the parameter ν_p accordingly. Thus the actual value of the concentration is open to calibration against the experimental data. Also, in most numerical simulations, the term $P\rho_0^{-2}\mathbf{R}$ is much larger than the unity tensors in (3.2) and (3.5). Therefore, in the theoretical development below we shall use the approximation

$$T_{\alpha\beta} \sim \nu_p P R_{\alpha\beta} / \tau \rho_0^2. \quad (3.6)$$

We note that the conformation tensor always appears rescaled by ρ_0^2 . For notational simplicity we will absorb ρ_0^2 into the definition of the conformation tensor, and keep the notation $R_{\alpha\beta}$ for the renormalized, dimensionless tensor.

Considering first homogeneous and isotropic turbulence, The FENE-P model can be used to demonstrate the Lumley scale discussed above. In homogeneous turbulence one measures the moments of the velocity difference across a length scale r' , and in particular the second order structure function

$$S_2(r') \equiv \langle \{ [\mathbf{U}(\mathbf{r} + \mathbf{r}', t) - \mathbf{U}(\mathbf{r}, t)] \cdot \frac{\mathbf{r}'}{r'} \}^2 \rangle, \quad (3.7)$$

where the average $\langle \dots \rangle$ is performed over space and time. This quantity changes when the simulations are done with the Navier-Stokes equations on the one hand and with the FENE-P equations on the other, see (De-Angelis et al., 2005)). The polymers decrease the amount of energy at small scales. The reduction starts exactly at the theoretical estimate of the Lumley scale, shown with an arrow in Fig. 6. A more detailed analysis of the energy transfer (De-Angelis et al., 2005) shows that energy flows from large to small scales and at the Lumley scale a significant amount of energy is transferred to the potential energy of the polymers by increasing $R_{\gamma\gamma}$. This energy is eventually dissipated when the polymer relax their length back to equilibrium. In contradistinction to the picture offered by de-Gennes (1990), simulations indicate that the energy *never* goes back from the polymers to the flow; the only thing that the polymers can do is to increase the dissipation. This is a crucial statement underlying again the challenge of developing a consistent theory of drag reduction. In isotropic and homogeneous conditions the effect of polymer is just to lower the effective Reynolds number which, of course, cannot explain drag reduction.

The FENE-P equations were also simulated on the computer in a channel or pipe geometry, reproducing the phenomenon of drag reduction found in experiments (Benzi et al., 2006; Dimitropoulos et al., 1998, 2005; Ptasinski et al., 2001). The most basic characteristic of the phenomenon is the increase of fluid throughput in the channel for the same pressure head, compared to

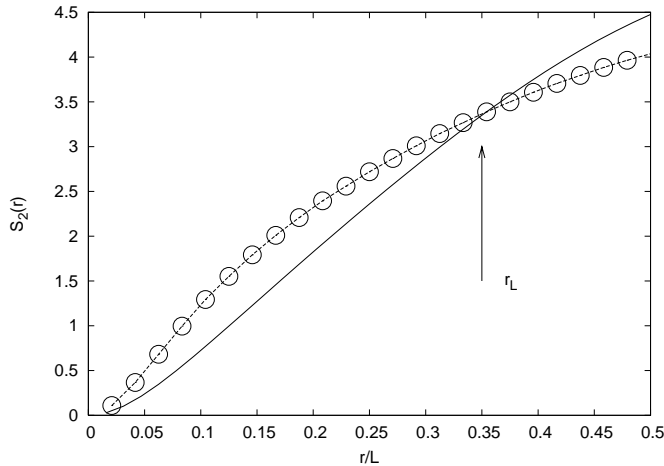


FIG. 6 Second order structure function $S_2(r)$ for homogeneous and isotropic turbulence. Two cases are represented: with polymers (line with symbols) and without polymer (dashed line). The Lumley scale is indicated by an arrow. The numerical simulations with polymers is performed using a 128^3 resolution with periodic boundary conditions. The energy content for scales below the Lumley scale is reduced indicating a significant energy transfer from the velocity field to the polymer elastic energy.

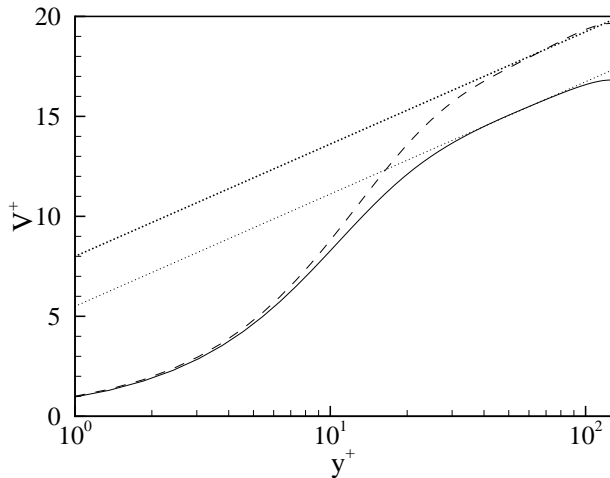


FIG. 7 Mean velocity profiles for the Newtonian and for the viscoelastic simulations with $Re = 125$ (Benzi et al., 2006). Solid line: Newtonian. Dashed line: Viscoelastic. The straight lines represent a log-law with the classical von Kármán slope. Notice that in this simulation the modest Reynolds number results in an elastic layer in the region $y^+ \leq 20$.

the Newtonian flow. This phenomenon is demonstrated in Fig. 7. As one can see the simulation is limited compared to experiments; the Reynolds number is relatively low, and the MDR is not attained. Nevertheless the phenomenon is there. At any rate, once we are convinced that the FENE-P model exhibits drag reduction,

it must also reproduce the universal properties of the phenomenon, and in particular the MDR. We will show that this is indeed the case, but that also all the cross-over non-universal phenomena can be understood using this model. If we were not interested in the cross-over phenomena we could use directly the large concentration limit of the FENE-P model, which is the limit $P = 1$ where the model identifies with the harmonic Dumbbell-model known also as the Oldroyd-B model.

B. Derivation of the MDR

In this section we review the theory that shows how the new log-law (1.6) comes about when the polymers are added to the flow. In the next section we explain why this law is universal and estimate the parameters from first principles.

As before, we proceed by taking the long time average of Eq. (3.4), and integrating the resulting equation along the y coordinate. This produces an exact equation for the momentum balance:

$$W + \nu_0 S + \frac{\nu_p}{\tau} \langle PR_{xy} \rangle (y) = p'(L - y). \quad (3.8)$$

The interpretation of this equation is as before, but we have a new term which is the rate at which momentum is transferred to the polymers. Near the wall it is again permissible to neglect the term $p'y$ on the RHS for $y \ll L$. One should not be surprised with the form of Eq. (3.8), the new term could only be the one that is appearing there, since it must have an $x-y$ symmetry, and it simply stems from the additional stress tensor appearing in Eq. (3.4). The derivation of the energy balance equation is more involved, and had been described in great detail in (Benzi et al., 2006; L'vov et al., 2005a). The final form of the equation is

$$a\nu_0 \frac{K}{y^2} + b \frac{K^{3/2}}{y} + c_4 \nu_p \langle R_{yy} \rangle \frac{K(y)}{y^2} = WS, \quad (3.9)$$

where c_4 is a dimensionless coefficient of the order of unity. This equation is in its final form, ready to be analyzed further. Equation (3.8) needs to be specialized to the vicinity of the MDR, which is only obtained when the concentration c_p of the polymers is sufficiently high, when Re is sufficiently high, but also when the Deborah number De is sufficiently high. In (Benzi et al., 2006; L'vov et al., 2005a) it was shown that when these conditions are met,

$$\langle PR_{xy} \rangle = c_1 \langle R_{yy} \rangle S \tau, \quad (3.10)$$

where c_1 is another dimensionless coefficient of the order of unity. Using this result in Eq. (3.8) we end up with the momentum balance equation

$$W(y) + \nu_0 S(y) + c_1 \nu_p \langle R_{yy} \rangle (y) S(y) = p'L, \quad y \ll L. \quad (3.11)$$

The substitution (3.10) is so important for what follows that we dwell on it a bit further. When the conditions discussed above are all met, the polymers tend to be stretched and well aligned with the flow, such that the xx component of the conformation tensor must be much larger than the xy component, with the yy component being the smallest, tending to zero with $\mathcal{De} \rightarrow \infty$. Since \mathcal{De} is the only dimensionless number that can relate the various components of $\langle R_{ij} \rangle$, we expect that $\langle R_{xx} \rangle \sim \mathcal{De} \langle R_{xy} \rangle$ and $\langle R_{xy} \rangle \sim \mathcal{De} \langle R_{yy} \rangle$. Indeed, a calculation (L'vov et al., 2005a) shows that in the limit $\mathcal{De} \rightarrow \infty$ the conformation tensor attains the following universal form:

$$\langle \mathbf{R} \rangle \simeq \langle R_{yy} \rangle \begin{pmatrix} 2\mathcal{De}^2 & \mathcal{De} & 0 \\ \mathcal{De} & 1 & 0 \\ 0 & 0 & C \end{pmatrix} \quad \text{for } \mathcal{De} \gg 1, \quad (3.12)$$

where C is of the order of unity. We conclude that R_{xx} is much larger than any other component of the conformation tensor, but it plays no direct role in the phenomenon of drag reduction. Rather, R_{yy} which is very much smaller, is the most important component from our point of view. We can thus rewrite the two balance equations derived here in the suggestive form:

$$\nu(y)S + W = p'L, \quad (3.13)$$

$$\tilde{a}\nu(y)\frac{K}{y^2} + b\frac{K^{3/2}}{y} = WS, \quad (3.14)$$

where $\tilde{a} = ac_4/c_1$ and the ‘‘effective viscosity’’ $\nu(y)$ is being identified as

$$\nu(y) \equiv \nu_0 + c_1 \nu_p \langle R_{yy} \rangle. \quad (3.15)$$

Exactly like in the Newtonian theory one needs to add a phenomenological relation between $W(y)$ and $K(y)$ which holds in the elastic layer,

$$W(y) = c_v^2 K(y), \quad (3.16)$$

with c_v an unknown coefficient of the order of unity.

At this point one asserts that the ‘dressed’ viscous term dominates the inertial term on the LHS of the balance equations (3.13) and (3.14). From the first of these we estimate $\nu(y) \sim p'L/S(y)$. Plugged into the second of these equations this leads, together with Eq. (2.6) to $S(y) = \text{Const.}/y$, where Const. is a combination of the unknown coefficients appearing in these equations, and therefore is itself an unknown coefficient of the order of unity. The important thing is that the theory predicts a new log-law for $V(y)$, the slope of which we will shown to be universal in the next Subsection. Before we do so it is important to realize that if $S(y) = \text{Const.}/y$, our analysis indicates that the effective viscosity $\nu(y)$ must grow outside the viscous layer linearly in y , $\nu(y) \sim y$. If we make the self-consistent assumption that ν_0 is negligible in the log-law region compared to $\nu_p \langle R_{yy} \rangle$, then this prediction appears in contradiction with what is known about the stretching of polymers in channel geometry, where it had

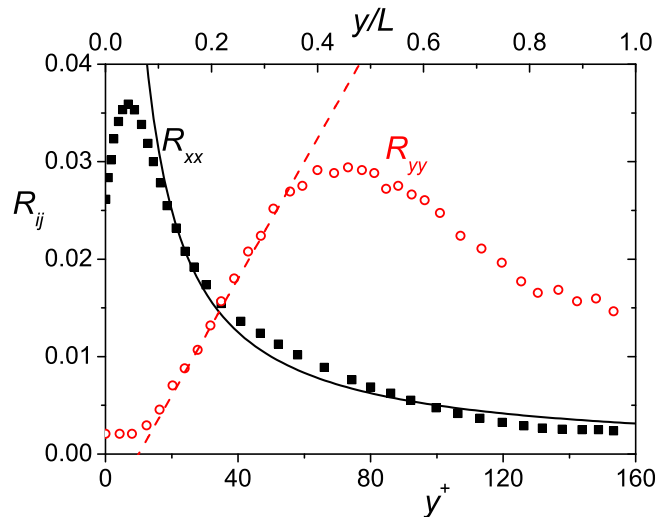


FIG. 8 Comparison of the DNS data Ref. (Sibila and Baron, 2002) for the mean profiles of R_{xx} and $10 \times R_{yy}$, the components of the dimensionless conformation tensor, with analytical predictions. In our notation $\Pi_0^{ij} \equiv \nu_{0p} R_{\max}^2 R_{ij} / (\tau_p R_{\text{eq}}^2)$. Black squares: DNS data for the streamwise diagonal component R_{xx} , that according to our theory has to decrease as $1/y^+$ with the distance to the wall. Black solid line: the function $1/y^+$. Red empty circles: DNS data for the wall-normal component $10R_{yy}$, for which we predicted a linear increase with y^+ in the log-law turbulent region. Red dashed line - linear dependence, $\propto y^+$.

been measured that the extent of stretching *decreases* as a function of the distance from the wall. The apparent contradiction evaporates when we recall that the amount of stretching is dominated by R_{xx} which is indeed decreasing. To see this note that Eq. (3.12) predicts that $R_{xx} \approx 2\mathcal{De}^2 R_{yy} \propto 1/y$. At the same time R_{yy} increases linearly in y . Both predictions agree with what is observed in simulations, see Fig. 8.

The simplicity of the resulting theory, and the correlation between a linear viscosity profile and the phenomenon of drag reduction raises the natural question, is it enough to have a viscosity that rises linearly as the function of the distance from the wall to cause drag reduction? To answer this question one can simulate the Navier-Stokes equations with proper viscosity profiles (discussed below) and show that the results are in semi-quantitative agreement with the corresponding full FENE-P DNS. Such simulations were done (De-Angelis et al., 2004) in a domain $2\pi L \times 2L \times 1.2\pi L$, with periodic boundary conditions in the streamwise and spanwise directions, and with no slip conditions on the walls that were separated by $2L$ in the wall-normal direction. An imposed mass flux and the same Newtonian initial conditions were used. The Reynolds number Re (computed with the centerline velocity) was 6000 in all the runs. The y dependence of the scalar effective viscosity was close to being piece-wise linear along the channel height, namely $\nu = \nu_0$ for $y \leq y_1$, a linear portion with a prescribed slope for $y_1 < y \leq y_2$, and again a constant value

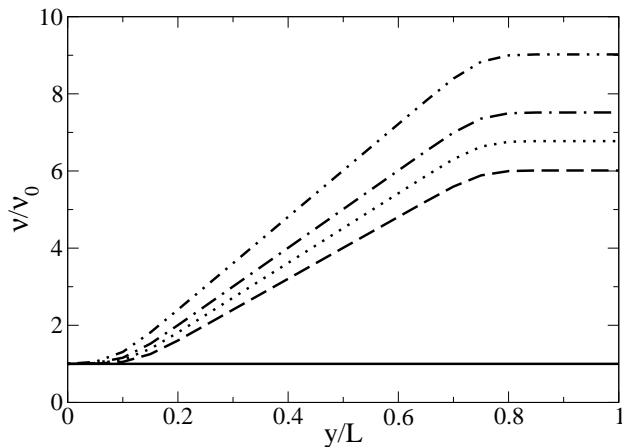


FIG. 9 The Newtonian viscosity profile and four examples of close to linear viscosity profiles employed in the numerical simulations. Solid line: run N, ---: run R, \cdots : run S, - · - ·: T, - - - -: run U.

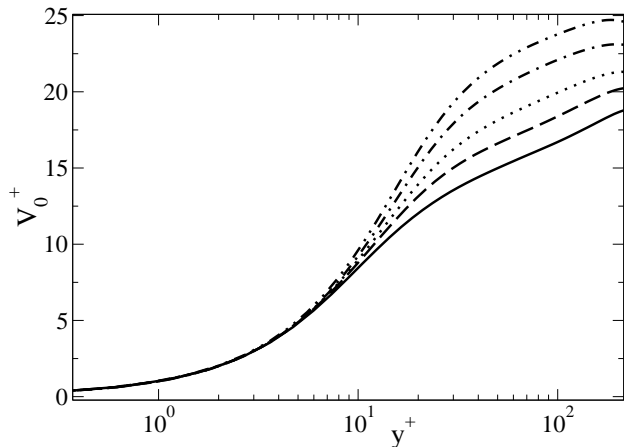


FIG. 10 The reduced mean velocity as a function of the reduced distance from the wall. The line types correspond to those used in Fig. 9.

for $y_2 < y < L$. For numerical stability this profile was smoothed out as shown in Fig. 9. Included in the figure is the flat viscosity profile of the standard Newtonian flow. In Fig. 10 we show the resulting profiles of $V_0^+(y)$ vs. y^+ . The line types are chosen to correspond to those used in Fig. 9. The *decrease* of the drag with the *increase* of the slope of the viscosity profiles is obvious. Since the slopes of the viscosity profiles are smaller than needed to achieve the MDR asymptote for the corresponding $\mathcal{R}e$, the drag reduction occurs only in the near-wall region and the Newtonian plugs are clearly visible.

The conclusion of these simulations appears to be that one can increase the slope of the linear viscosity profile and gain further drag reduction. The natural question that comes to mind is whether this can be done without limit such as to reduce the drag to zero. Of course this

would not be possible, and here lies the clue for understanding the universality of the MDR.

C. The universality of the MDR: theory

The crucial new insight that will explain the universality of the MDR and furnish the basis for its calculation is that **the MDR is a marginal flow state of wall-bounded turbulence**: attempting to increase $S(y)$ beyond the MDR results in the collapse of the turbulent solutions in favor of a stable laminar solution with $W = 0$ (Benzi et al., 2005a). As such, the MDR is universal by definition, and the only question is whether a polymer (or other additive) can supply the particular effective viscosity $\nu(y)$ that drives Eqs. (3.13) and (3.14) to attain the marginal solution that maximizes the velocity profile. We expect that the same marginal state will exist in numerical solutions of the Navier-Stokes equations furnished with a y -dependent viscosity $\nu(y)$. There will be no turbulent solutions with velocity profiles higher than the MDR.

To see this explicitly, we first rewrite the balance equations in wall units. For constant viscosity [i.e. $\nu(y) \equiv \nu_0$], Eqs. (3.13)-(2.6) form a closed set of equations for $S^+ \equiv S\nu_0/(p'L)$ and $W^+ \equiv W/p'L$ in terms of two dimensionless constant $\delta^+ \equiv a\sqrt{K/W}$ (the thickness of the viscous boundary layer) and $\kappa_\kappa \equiv b/c_N^3$ (the Von Karman constant). Newtonian experiments and simulations agree well with a fit using $\delta^+ \sim 6$ and $\kappa_\kappa \sim 0.436$ (see the black continuous line in Fig. 2 which shows the mean velocity profile using these very constants). Once the effective viscosity $\nu(y)$ is no longer constant we expect c_N to change ($c_N \rightarrow c_v$) and consequently the two dimensionless constants will change as well. We will denote the new constants as Δ and κ_c respectively. Clearly one must require that for $\nu(y)/\nu_0 \rightarrow 1$, $\Delta \rightarrow \delta^+$ and $\kappa_c \rightarrow \kappa_\kappa$. The balance equations are now written as (Benzi et al., 2005a):

$$\nu^+(y^+)S^+(y^+) + W^+(y^+) = 1, \quad (3.17)$$

$$\nu^+(y^+)\frac{\Delta^2}{y^{+2}} + \frac{\sqrt{W^+}}{\kappa_c y^+} = S^+, \quad (3.18)$$

where $\nu^+(y^+) \equiv \nu(y^+)/\nu_0$. Substituting now S^+ from Eq. (3.17) into Eq. (3.18) leads to a quadratic equation for $\sqrt{W^+}$. This equation has as a zero solution for W^+ (laminar solution) as long as $\nu^+(y^+)\Delta/y^+ = 1$. Turbulent solutions are possible only when $\nu^+(y^+)\Delta/y^+ < 1$. Thus at the edge of existence of turbulent solutions we find $\nu^+ \propto y^+$ for $y^+ \gg 1$. This is not surprising, since it was observed above that the MDR solution is consistent with an effective viscosity which is asymptotically linear in y^+ . It is therefore sufficient to seek the edge solution of the velocity profile with respect to linear viscosity profiles, and we rewrite Eqs. (3.17) and (3.18) with an effective viscosity that depends linearly on y^+ outside the

boundary layer of thickness δ^+ :

$$[1 + \alpha(y^+ - \delta^+)]S^+ + W^+ = 1, \quad (3.19)$$

$$[1 + \alpha(y^+ - \delta^+)]\frac{\Delta^2(\alpha)}{y^{+2}} + \frac{\sqrt{W^+}}{\kappa_c y^+} = S^+. \quad (3.20)$$

We now endow Δ with an explicit dependence on the slope of the effective viscosity $\nu^+(y)$, $\Delta = \Delta(\alpha)$. Since drag reduction must involve a decrease in W , we expect the ratio a^2K/W to depend on α , with the constraint that $\Delta(\alpha) \rightarrow \delta^+$ when $\alpha \rightarrow 0$. Although Δ , δ^+ and α are all dimensionless quantities, physically Δ and δ^+ represent (viscous) length scales (for the linear viscosity profile and for the Newtonian case respectively) while α^{-1} is the scale associated to the slope of the linear viscosity profile. It follows that $\alpha\delta^+$ is dimensionless even in the original physical units. It is thus natural to present $\Delta(\alpha)$ in terms of a dimensionless scaling function $f(x)$,

$$\Delta(\alpha) = \delta^+ f(\alpha\delta^+). \quad (3.21)$$

Obviously, $f(0) = 1$. In the Appendix we show that the balance equations (3.19) and (3.20) (with the prescribed form of the effective viscosity profile) have a non-trivial symmetry that leaves them invariant under rescaling of the wall units. This symmetry dictates the function $\Delta(\alpha)$ in the form

$$\Delta(\alpha) = \frac{\delta^+}{1 - \alpha\delta^+}. \quad (3.22)$$

Armed with this knowledge we can now find the maximal possible velocity far away from the wall, $y^+ \gg \delta^+$. There the balance equations simplify to

$$\alpha y^+ S^+ + W^+ = 1, \quad (3.23)$$

$$\alpha \Delta^2(\alpha) + \sqrt{W^+}/\kappa_c = y^+ S^+. \quad (3.24)$$

These equations have the y^+ -independent solution for $\sqrt{W^+}$ and $y^+ S^+$:

$$\begin{aligned} \sqrt{W^+} &= -\frac{\alpha}{2\kappa_c} + \sqrt{\left(\frac{\alpha}{2\kappa_c}\right)^2 + 1 - \alpha^2 \Delta^2(\alpha)}, \\ y^+ S^+ &= \alpha \Delta^2(\alpha) + \sqrt{W^+}/\kappa_c. \end{aligned} \quad (3.25)$$

By using equation (3.25), (see Fig. 11), we obtain that the edge solution ($W^+ \rightarrow 0$) corresponds to the supremum of $y^+ S^+$, which happens precisely when $\alpha = 1/\Delta(\alpha)$. Using Eq. (3.22) we find the solution $\alpha = \alpha_m = 1/2\delta^+$. Then $y^+ S^+ = \Delta(\alpha_m)$, giving $\kappa_v^{-1} = 2\delta^+$. Using the estimate $\delta^+ \approx 6$ we get the final prediction for the MDR. Using Eq. (1.6) with $\kappa_v^{-1} = 12$, we get

$$V^+(y^+) \approx 12 \ln y^+ - 17.8. \quad (3.26)$$

This result is in close agreement with the empirical law (1.5) proposed by Virk. The value of the intercept on the RHS of Eq. (3.26) follows from Eq. (1.6) which is based on matching the viscous solution to the MDR log-law in

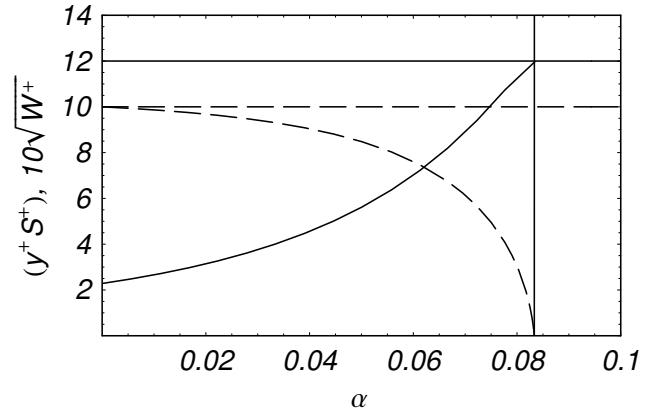


FIG. 11 The solution for $10\sqrt{W^+}$ (dashed line) and $y^+ S^+$ (solid line) in the asymptotic region $y^+ \gg \delta^+$, as a function of α . The vertical solid line $\alpha = 1/2\delta^+ = 1/12$ which is the edge of turbulent solutions; Since $\sqrt{W^+}$ changes sign here, to the right of this line there are only laminar states. The horizontal solid line indicates the highest attainable value of the slope of the MDR logarithmic law $1/\kappa_v = 12$.

(L'vov et al., 2004). We now also have the deep justification for this matching: the MDR is basically a laminar solution that can match smoothly with the viscous sub-layer, with continuous derivative. This is not possible for the von Kármán log-law which represents fully turbulent solutions. Note that the numbers appearing in Virk's law correspond to $\delta^+ = 5.85$, which is well within the error-bar on the value of this Newtonian parameter. Note that we can easily predict where the asymptotic law turns into the viscous layer upon the approach to the wall. We can consider an infinitesimal W^+ and solve Eqs. (3.17) and (3.18) for S^+ and the viscosity profile. The result, as before, is $\nu^+(y) = \Delta(\alpha_m)y^+$. Since the effective viscosity cannot fall below the Newtonian limit $\nu^+ = 1$ we see that the MDR cannot go below $y^+ = \Delta(\alpha_m) = 2\delta^+$. We thus expect an extension of the viscous layer by a factor of 2, in very good agreement with the experimental data.

Note that the result $W^+ = 0$ should not be interpreted as $W = 0$. The difference between the two objects is the factor of $p'L$, $W = p' L W^+$. Since the MDR is reached asymptotically as $\mathcal{R}e \rightarrow \infty$, there is enough turbulence at this state to stretch the polymers to supply the needed effective viscosity. Indeed our discussion is in close correspondence with the experimental remark by Virk (Virk, 1975) that close to the MDR asymptote the flow appears laminar.

In summary, the main message of this section is that the added polymers endow the fluid with an effective viscosity $\nu(y)$ instead of ν_0 . There exists a profile of $\nu(y)$ that results in a maximal possible velocity profile at the edge of existence of turbulent solutions. That profile is the prediction for the MDR. In particular we offer a prediction for simulations: direct numerical simulations of the Navier-Stokes equations in wall bounded geometries, endowed with a linear viscosity profile (De-Angelis et al.,

2004), will not be able to support turbulent solutions when the slope of the viscosity profile exceeds the critical value that is in correspondence with the slope of the MDR.

IV. THE “ADDITIVE EQUIVALENCE”: THE MDR OF ROD-LIKE POLYMERS

In this section we address the experimental finding that *rigid rod-like* polymers appear to exhibit the same MDR (1.6) as flexible polymers (Virk et al., 1997). Since the bare equations of motion of rod-like polymers differ quite significantly from those of flexible polymers, one needs to examine the issue carefully to understand this universality, which was termed by Virk “Additive Equivalence”. We will see that the point is that in spite of the different basic equations, when the conditions allow attainment of the MDR, the balance equations for momentum and energy are identical in form to those of the flexible polymers (Benzi et al., 2005b; Ching et al., 2006). The differences between the two types of polymers arise when we consider how the MDR is approached, and cross-overs back to the Newtonian plugs, all issues that are taken up below.

A. Hydrodynamics with rod-like polymers

The equation for the incompressible velocity field $\mathbf{U}(\mathbf{r}, t)$ in the presence of rod-like polymers has a form isomorphic to Eq. (3.4)

$$\frac{\partial \mathbf{U}}{\partial t} + \mathbf{U} \cdot \nabla \mathbf{U} = \nu_0 \Delta \mathbf{U} - \nabla p + \nabla \cdot \boldsymbol{\sigma}, \quad (4.1)$$

but with another $\boldsymbol{\sigma} \Rightarrow \sigma_{ab}$ playing the role of an extra stress tensor caused by the polymers.

The calculation of the tensor $\boldsymbol{\sigma}$ for rigid rods is offered in the literature (Doi and Edwards, 1988), subject to the realistic assumptions that the rod-like polymers are mass-less and having no inertia. In other words, the rod-like polymers are assumed to be at all times in local rotational equilibrium with the velocity field. Thus the stress tensor does not have a contribution from the rotational fluctuations against the fluid, but rather only from the velocity variations along the rod-like object. Such variations lead to “skin friction”, and this is the only extra dissipative effect that is taken into account (Brenner, 1974; Hinch and Leal, 1975, 1976; Manhart, 2003). The result of these considerations is the following expression for the additional stress tensor:

$$\sigma_{ab} = 6\nu_p n_a n_b (n_i n_j \mathcal{S}_{ij}), \quad \text{rod-like polymers,} \quad (4.2)$$

where ν_p is the polymeric contribution to the viscosity at vanishingly small and time-independent shear; ν_p increases linearly with the polymer concentration, making it an appropriate measure for the polymer’s concentration. The other quantities in Eq. (4.2) are the velocity

gradient tensor

$$\mathcal{S}_{ab} = \partial U_a / \partial x_b, \quad (4.3)$$

and $\mathbf{n} \equiv \mathbf{n}(\mathbf{r}, t)$ is a unit ($\mathbf{n} \cdot \mathbf{n} \equiv 1$) director field that describe the polymer’s orientation. Notice, that for flexible polymers the equation (3.6) for T_{ab} is completely different from (4.2). The difference between Eqs. (4.2) and (3.6) for the additional stress tensor in the cases of rod-like and flexible polymers reflects their very different microscopic dynamics. For the flexible polymers the main source of interaction with the turbulent fluctuations is the stretching of the polymers by the fluctuating shear s . This is how energy is taken from the turbulent field, introducing an additional channel of dissipation without necessarily increasing the local gradient. In the rod-like polymer case the dissipation is only taken as the skin friction along the rod-like polymers. Having in mind all these differences it becomes even more astonishing that the macroscopic equations for the mechanical momentum and kinetic energy balances are isomorphic for the rod-like and flexible polymers, as is demonstrated below.

B. The balance equations and the MDR

Using Eq. (4.2) and Reynolds decomposition (2.1) we compute

$$\langle \sigma_{xy} \rangle = 6\nu_p \langle \mathcal{R}_{xy} \mathcal{R}_{ij} \mathcal{S}_{ij} \rangle = 6\nu_p [S \langle \mathcal{R}_{xy}^2 \rangle + \langle \mathcal{R}_{xy} \mathcal{R}_{ij} s_{ij} \rangle]. \quad (4.4)$$

Now we make use of the expected solution for the conformation tensor in the case of large mean shear. In such flows we expect a strong alignment of the rod-like polymers along the streamwise direction x . The director components n_y and n_z are then much smaller than $n_x \approx 1$. For large shear we can expand n_x according to

$$n_x = \sqrt{1 - n_y^2 - n_z^2} \approx 1 - \frac{1}{2}(n_y^2 + n_z^2). \quad (4.5)$$

This expansion allows us to express all products $\mathcal{R}_{ab} \mathcal{R}_{cd} = n_a n_b n_c n_d$ in terms that are linear in \mathcal{R} , up to third order terms in $n_y \sim n_z$. In particular

$$\mathcal{R}_{xx}^2 \approx 1 - 2(\mathcal{R}_{yy} + \mathcal{R}_{zz}), \quad \mathcal{R}_{xy}^2 \approx \mathcal{R}_{yy}. \quad (4.6)$$

With (4.6) the first term in the RHS of Eq. (4.4) can be estimated as

$$6\nu_p S \langle \mathcal{R}_{xy}^2 \rangle = \tilde{c}_1 \nu_p \langle \mathcal{R}_{yy} \rangle S, \quad \tilde{c}_1 \simeq 6. \quad (4.7)$$

The estimate of the second term on the RHS of Eq. (4.4) needs some further calculations which can be found in (Benzi et al., 2005b; Ching et al., 2006), with the result that it is of the same order as the first one. Finally we can present therefore the momentum balance equation in the form

$$\nu_0 S + c_1 \nu_p \langle \mathcal{R}_{yy} \rangle S + W = p' L. \quad (4.8)$$

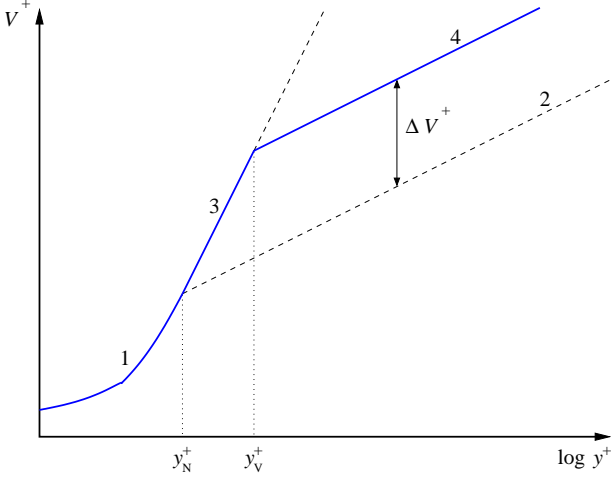


FIG. 12 Schematic mean velocity profiles. Region 1: $y^+ < y_N^+$, - viscous sublayer. Region 2: $y^+ > y_N^+$, - logarithmic layer for the turbulent Newtonian flow. Region 3: $y_N^+ < y^+ < y_V^+ = (1+Q)y_N^+$ - MDR asymptotic profile in the viscoelastic flow. Region 4: $y^+ > y_V^+$ - Newtonian plug in the viscoelastic flow.

Another way of writing this result is in the form of an effective viscosity,

$$\nu(y)S + W = p'L, \quad (4.9)$$

where the effect of the rod-like polymers is included by the effective viscosity $\nu(y)$:

$$\nu(y) \equiv \nu_0 + c_1 \nu_p \langle R_{yy} \rangle. \quad (4.10)$$

We see that despite the very different microscopic stress tensors, the final momentum balance equation is the same for the flexible and the rod-like polymers. Additional calculations which can be found in (Benzi et al., 2005b) show that the energy balance equation also attains the precisely the same form as Eq. (3.14). Evidently this immediately translates, via the theory of the previous sections, to the same MDR by the same mechanism, and therefore the “additive equivalence”.

V. NON-UNIVERSAL ASPECTS OF DRAG REDUCTION: FLEXIBLE POLYMERS

In this section we return to the cross-over phenomena described in Subsect. I.B.2 and Subsect. I.B.3 and provide the theory (Benzi et al., 2004b) for their understanding. First we refer to the experimental data in Fig. 3.

A. The efficiency of drag reduction for flexible polymers

When there exist cross-overs back from the MDR to the Newtonian plugs the mean velocity profile in the flexible polymer case consists of three regions (Virk, 1975): a

viscous sublayer, a logarithmic elastic sublayer (region 3 in the Fig. 12) with the slope greater than the Newtonian one, Eq. (1.5), and a Newtonian plug (region 4). In the last region the velocity follows a log-law with the Newtonian slope, but with some velocity increment ΔV^+ :

$$V^+(y^+) = \kappa_K^{-1} \ln y^+ + B_K + \Delta V^+. \quad (5.1)$$

Note that we have simplified the diagram for the sake of this discussion: the three profiles Eqs. (1.2), (1.3), and (1.5) intercept at one point $y^+ = y_N^+ \simeq \kappa_V^{-1} \simeq 11.7 \approx 2\delta^+$. In reality the Newtonian log-law does not connect sharply with the viscous solution $V^+ = y^+$, but rather through a cross-over region of the order of δ^+ .

The increment ΔV^+ which determines the amount of drag reduction is in turn determined by the cross-over from the MDR to the Newtonian plug (see Fig. 12). We refer to this cross-over point as y_V^+ . To measure the quality of drag reduction one introduces (Benzi et al., 2004b) a dimensionless drag reduction parameter

$$Q \equiv \frac{y_V^+}{y_N^+} - 1. \quad (5.2)$$

The velocity increment ΔV^+ is related to this parameter as follows

$$\Delta V^+ = (\kappa_V^{-1} - \kappa_K^{-1}) \ln (y_V^+/y_N^+) = \beta \ln(1+Q). \quad (5.3)$$

Here $\beta \equiv \kappa_V^{-1} - \kappa_K^{-1} \simeq 9.4$. The Newtonian flow is then a limiting case of the viscoelastic flow corresponding to $Q = 0$.

The cross-over point y_V^+ is non-universal, depending on \mathcal{Re} , on the number of polymers per unit volume c_p , the chemical nature of the polymer, etc. According to the theory of the last Section, the total viscosity of the fluid $\nu_{\text{tot}}(y^+) = \nu_0 + \nu_p(y^+)$ [where $\nu_p(y^+)$ is the polymeric contribution to the viscosity which is proportional to $\langle R_{yy} \rangle$] is linear in y^+ in the MDR region:

$$\nu_{\text{tot}}(y^+) = \nu_0 y^+/y_N^+, \quad y_N^+ < y^+ < y_V^+. \quad (5.4)$$

When the concentration of polymers is small and \mathcal{Re} is large enough, *the cross-over to the Newtonian plug at y_V^+ occurs when the polymer stretching can no longer provide the necessary increase of the total fluid viscosity*. In other words, in that limit the cross-over is due to the finite extensibility of the polymer molecules. Obviously, the polymeric viscosity can not be greater than $\nu_{p \text{ max}}$ which is the viscosity of the fully stretched polymers. Thus the total viscosity is limited by $\nu_0 + \nu_{p \text{ max}}$. Equating $\nu_0 + \nu_{p \text{ max}}$ and $\nu_{\text{tot}}(y_V^+)$ gives us the cross-over position

$$y_V^+ = y_N^+ (\nu_0 + \nu_{p \text{ max}}) / \nu_0. \quad (5.5)$$

It follows from Eq. (5.2) that the drag reduction parameter is determined very simply by

$$Q = \nu_{p \text{ max}} / \nu_0, \quad c_p \text{ small, } \mathcal{Re} \text{ large}. \quad (5.6)$$

At this point we need to relate the maximum polymeric viscosity $\nu_{p \max}$ to the polymer properties. To this aim we estimate the energy dissipation due to a single, fully stretched, polymer molecule. In a reference frame co-moving with the polymer's center of mass the fluid velocity can be estimated as $u \simeq r \nabla u$ (the polymer's center of the mass moves with the fluid velocity due to negligible inertia of the molecule). The friction force exerted on the i -th monomer is estimated using Stokes law with δu_i being the velocity difference across a monomer,

$$F_i \simeq \rho_0 \nu_0 a \delta u_i = \rho_0 \nu_0 a r_i \nabla u, \quad (5.7)$$

where a is an effective hydrodynamic radius of one monomer (depending on the chemical composition), and r_i is the distance of the i -th monomer from the center of the mass. In a fully stretched state $r_i \simeq a i$ (the monomers are aligned along a line). The energy dissipation rate (per unit volume) is equal to the work performed by the external flow

$$\begin{aligned} -\frac{dE}{dt} &\simeq c_p \sum_{i=1}^{N_p} F_i \delta u_i \simeq \rho_0 \nu_0 a^3 c_p N_p^3 (\nabla u)^2 \\ &\equiv \rho_0 \nu_{p \max} (\nabla u)^2. \end{aligned} \quad (5.8)$$

We thus can estimate $\nu_{p \max}$:

$$\nu_{p \max} = \nu_0 a^3 c_p N_p^3. \quad (5.9)$$

Finally, the drag reduction parameter Q is given by

$$Q = a^3 c_p N_p^3 \quad c_p \text{ small, } \mathcal{R}e \text{ large}. \quad (5.10)$$

This is the central theoretical result of Benzi et al. (2004b), relating the concentration c_p and degree of polymerization N_p to the increment in mean velocity ΔV^+ via Eq. (5.3).

B. Drag reduction when polymers are degraded

The main experimental results which are of interest to us are summarized in Fig. 3. Note that in this experiment the flow geometry is rather complicated: with counter-rotating disks the *linear* velocity depends on the radius, and the local Reynolds number is a function of the radius. The drag reduction occurs however in a relatively small near-wall region, where the flow can be considered as a flow near the flat plate. Thus, one considers (Benzi et al., 2004b) an equivalent channel flow – with the same $\mathcal{R}e$ and a half width L of the order of height/radius of the cylinder. In this plane geometry the torques in (1.7) should be replaced by the pressure gradients $p'_{N,V}$:

$$\%DR = \frac{p'_N - p'_V}{p'_N} \times 100. \quad (5.11)$$

In order to relate %DR with the drag reduction parameter Q , one re-writes Eq. (5.1) in natural units

$$V(y) = \sqrt{p'L} \left[\kappa_K^{-1} \ln \left(y \sqrt{p'L} / \nu_0 \right) + B_K + \Delta V^+ \right]. \quad (5.12)$$

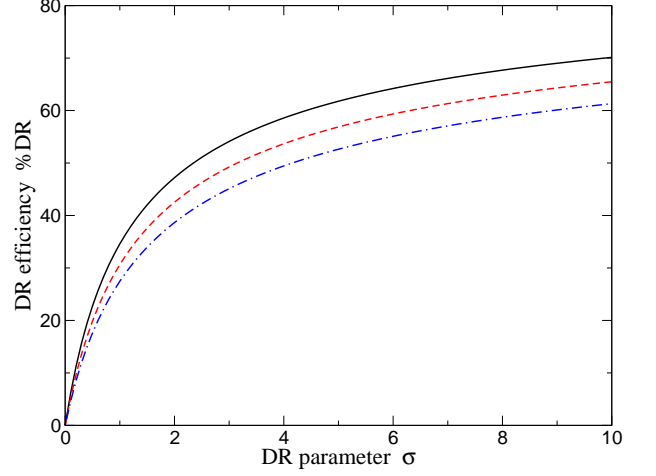


FIG. 13 Drag reduction efficiency %DR as function of the drag reducing parameter Q for different centerline Reynolds numbers Re : 1.2×10^5 , 1.2×10^6 , and 1.2×10^7 (from top to bottom).

To find the degree of drag reduction one computes p'_V and p'_N keeping the centerline velocity $V(L)$ constant. Defining the centerline Reynolds number as Re , we rewrite

$$Re \equiv \frac{V(L)L}{\nu_0} = \mathcal{R}e \left[\kappa_K^{-1} \ln \mathcal{R}e + B_K + \Delta V^+ \right]. \quad (5.13)$$

This equation implicitly determines the pressure gradient and therefore the %DR as a function of Q and Re . The set of Eqs. (5.3) and (5.13) is readily solved numerically, and the solution for three different values of Re is shown in Fig. 13. The middle curve corresponds to $Re = 1.2 \times 10^6$, which coincides with the experimental conditions (Choi et al., 2002). One sees, however, that the dependence of %DR on Re is rather weak. One important consequence of the solutions shown in Fig. 13 is that for small Q (actually for $Q \leq 0.5$ or %DR ≤ 20), %DR is approximately a linear function of Q . The experiments (Choi et al., 2002) lie entirely within this linear regime, in which we can linearize Eq. (5.13) in ΔV^+ , solve once for p'_V and once for p'_N (using $\Delta V^+ = 0$). Computing Eq. (5.11) we find an approximate solution for the %DR:

$$\%DR = \frac{2\beta Q}{\kappa_K^{-1} \ln(\mathcal{R}e_N) + B_K} \times 100. \quad (5.14)$$

Here $\mathcal{R}e_N$ is the friction Reynolds number for the Newtonian flow, i.e. the solution of Eq. (5.13) for $\Delta V^+ = 0$.

It is interesting to note, that while the %DR depends on the Reynolds number, the ratio of different %DR's does not [to $O(Q)$]:

$$\frac{\%DR^{(1)}}{\%DR^{(2)}} = \frac{Q^{(1)}}{Q^{(2)}} = \frac{\nu_{p \max}^{(1)}}{\nu_{p \max}^{(2)}}. \quad (5.15)$$

This result, together with Eq. (5.9), rationalizes completely the experimental finding of (Choi et al., 2002)

summarized in Fig. 3. During the DNA degradation, the concentration of polymers increases by a factor of 2, while the number of monomers N_p decreases by the same factor. This means that %DR should decrease by a factor of 4, as is indeed the case.

The experimental results pertain to high Re and small c_p , where we can assert that *the cross-over results from exhausting the stretching of the polymers such that the maximal available viscosity is achieved*. In the linear regime that pertains to this experiment the degradation has a maximal effect on the quality of drag reduction Q , leading to the precise factor of 4 in the results shown in Fig. 3. Larger values of the concentration of DNA will exceed the linear regime as is predicted by Fig. 13; then the degradation is expected to have a smaller influence on the drag reduction efficacy. It is worthwhile to test the predictions of this theory also in the nonlinear regime.

C. Other mechanism for cross-over

Having any reasonable model of polymer-laden flows at our disposal we can address other possibilities for the saturation of drag reduction. We expect a cross-over from the MDR asymptote back to the Newtonian plug when the basic assumptions on the relative importance of the various terms in the balance equations lose their validity, i.e. when (i) turbulent momentum flux W becomes comparable with the total momentum flux $p'L$, or when (ii) turbulent energy flux $bK^{3/2}/y$ becomes of the same order as turbulent energy production WS . In fact it was shown (Benzi et al., 2006) using the FENE-P model that both these conditions give the same cross-over point

$$y_v \simeq \frac{\tau\sqrt{p'L}}{\langle P \rangle}. \quad (5.16)$$

Note that $\tilde{\tau}(y) \equiv \tau/\langle P(y) \rangle$ is the effective non-linear polymer relaxation time. Therefore condition (5.16) can be also rewritten as

$$S(y_v)\tilde{\tau}(y_v) \simeq 1. \quad (5.17)$$

In writing this equation we use the fact that the cross-over point belongs also to the edge of the Newtonian plug where $S(y) \approx \sqrt{p'L}/y$. The LHS of this equation is simply the *local Deborah number* (product of local mean shear and local effective polymer relaxation time). Thus, *the cross-over to the Newtonian plug occurs at the point, where the local Deborah number decreases to ~ 1* . We expect that this result is correct for any model of elastic polymers, not only for the FENE-P model considered here.

To understand how the cross-over point y_v depends on the polymer concentration and other parameters, one needs to estimate mean value of the Peterlin function $\langle P \rangle$. Following Benzi et al. (2006) we estimate the value of $\langle P \rangle$ as

$$\langle P \rangle = \frac{1}{1 - \gamma\langle R \rangle}, \quad (5.18)$$

where $\langle R \rangle = \langle R_{xx} + R_{yy} + R_{zz} \rangle \sim \langle R_{xx} + 2R_{yy} \rangle$ and $\gamma \sim 1/\rho_m^2$ (for simplicity we disregard ρ_0). We know from before that

$$\langle R_{xx} \rangle \simeq (S\tilde{\tau})^2 \langle R_{yy} \rangle \quad (5.19)$$

and therefore at the cross-over point (5.17)

$$\langle R_{xx} \rangle \simeq \langle R_{yy} \rangle, \quad \langle R \rangle \simeq \langle R_{yy} \rangle.$$

The dependence of $\langle R_{yy} \rangle$ on y in the MDR region follows from Eqs. (3.11), since

$$\langle R_{yy} \rangle \simeq \frac{y\sqrt{p'L}}{\nu_p}.$$

Then at the cross-over point $y = y_v$:

$$\langle P \rangle \simeq \frac{1}{1 - \gamma y_v \sqrt{p'L}/\nu_p}.$$

Substituting this estimate into (5.16) gives the final result

$$y_v = \frac{C\tau\sqrt{p'L}}{1 + \gamma p'L\tau/\nu_p}. \quad (5.20)$$

Here C is constant of the order of unity. Finally, introducing dimensionless concentration of polymers

$$\tilde{c}_p \equiv \frac{\nu_p}{\gamma\nu_0}, \quad (5.21)$$

one can write denominator in Eq. (5.20) as

$$1 + \frac{\gamma p'L\tau}{\nu_p} = 1 + \frac{1}{\tilde{c}_p} \frac{p'L\tau}{\nu_0} = 1 + \frac{\mathcal{D}e}{\tilde{c}_p},$$

where

$$\mathcal{D}e \equiv \frac{p'L\tau}{\nu_0} \quad (5.22)$$

is the (global) Deborah number. Then for the dimensionless cross-over point $y_v^+ \equiv y_v\sqrt{p'L}/\nu_0$ one obtains

$$y_v^+ = \frac{C\mathcal{D}e}{1 + \mathcal{D}e/\tilde{c}_p}. \quad (5.23)$$

This prediction can be put to direct test when \tilde{c}_p is very large, or equivalently in the Oldroyd B model where $P \equiv 1$ (Benzi et al., 2004a). Indeed, in numerical simulations when the Weissenberg number was changed systematically, cf. (Yu et al., 2001), one observes the cross-over to depend on $\mathcal{D}e$ in a manner consistent with Eq. (5.23). The other limit when \tilde{c}_p is very small is in agreement with the linear dependence on \tilde{c}_p predicted in Eq. (5.10).

We can thus reach conclusions about the saturation of drag reduction in various limits of the experimental conditions, in agreement with experiments and simulations.

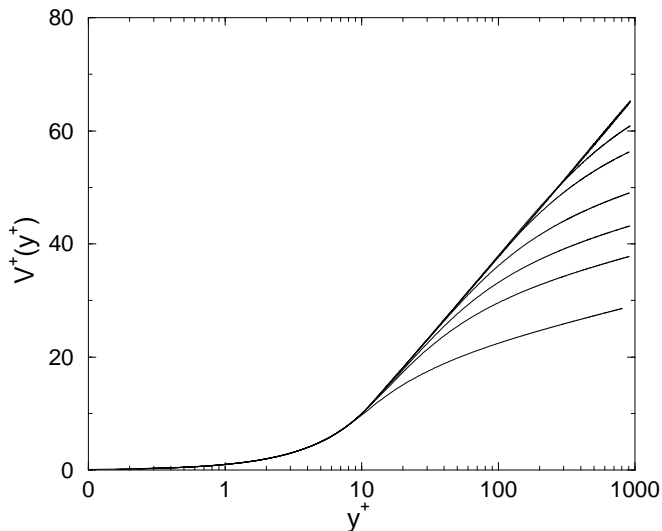


FIG. 14 The mean velocity profiles for flexible polymer additives with $\tilde{\nu} = 1, 5, 10, 20, 50, 100$ and 500 from below to above. Note that the profile follows the MDR until it crosses over back to the Newtonian plug.

VI. CROSS-OVER PHENOMENA WITH ROD-LIKE POLYMERS

A. The attainment of the MDR as a function of concentration

At this point we return to the different way that the MDR is approached by flexible and rod-like polymers when the concentration of the polymer is increased. As discussed above, in the case of flexible polymers the MDR is followed until the cross-over point y_v^+ that was discussed already in great detail. The rod-like polymers attain the MDR only asymptotically, and for intermediate values of the concentration the mean velocity profile increase gradually from the von Kármán log-law to the MDR log-law.

This difference can be fully understood in the context of the present theory. The detailed calculation addressing this issue was presented in (Ching et al., 2006). The results of the calculation, presented as the mean velocity profiles for increasing concentration of the two types of polymers are shown in Figs. 14 and 15. The reader should note the difference between these profiles as a function of the polymer concentration. While the flexible polymer case exhibits the feature (Virk et al., 1997; ?) that the velocity profile adheres to the MDR until a cross-over to the Newtonian plug is realized, the rod-like case presents a “fan” of profiles which only asymptotically reach the MDR. We also notice that the flexible polymer matches the MDR faithfully for relatively low values of $\tilde{\nu} \equiv \nu_p/\nu_0$, whereas the rod-like case attains the MDR only for much higher values of $\tilde{\nu}$. This result is in agreement with the experimental finding in (Bonn et al., 2005; Wagner et al., 2003) that the flexible polymer is a

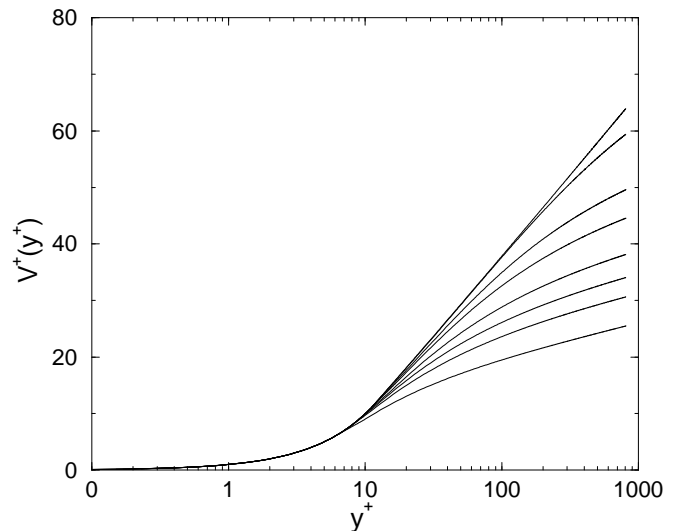


FIG. 15 The mean velocity profile for rod-like polymer additives with $\tilde{\nu} = 1, 5, 10, 20, 50, 100, 500, 1000, 5000$ and 10000 from below to above. Note the typical behavior expected for rod-like polymers, i.e. that the profile diverges from the von Kármán log-law, reaching the MDR only asymptotically.

better drag reducer than the rod-like analogue.

The calculation of (Ching et al., 2006) allows a parameter-free estimate of the cross-over points y_v^+ from the MDR to the “newtonian plug” in the case of flexible polymers. The resulting estimate reads

$$y_v^+ = 12 + \tilde{\nu}\sqrt{0.1}. \quad (6.1)$$

These estimates agrees well with the numerical results in Fig. 14. No such simple calculation is available for the case of the rod-like polymers since there is no clear point of departure for small $\tilde{\nu}$.

We should note that the higher efficacy of flexible polymers cannot be easily related to their elongational viscosity as measured in laminar flows. In some studies (Bonn et al., 2005; den Toonder et al., 1995; Wagner et al., 2003) it was proposed that there is a correlation between the elongational viscosity measured in laminar flows and the drag reduction measured in turbulent flows. We find here that flexible polymers do better in turbulent flows due to their contribution to the effective shear viscosity, and their improved capability in drag reduction stems simply from their ability to stretch, something that rod-like polymers cannot do.

B. Cross-over phenomena as a function of the Reynolds number

Finally, we address the drag enhancement by rod-like polymers when the values of \mathcal{Re} are too small, see Fig. 5. The strategy of Amarouchene et al. (2007) is to develop an approximate formula for the effective viscosity in the

case of rod-like polymers that interpolates properly between low and high values of \mathcal{Re} . For that purpose we remind the reader of the high \mathcal{Re} form of ν_{eff} , derive the form for low value of \mathcal{Re} , and then offer an interpolation formula.

Even for intermediate values of \mathcal{Re} one cannot neglect y in the production term $p'(L-y)$ in the momentum balance equation. Keeping this term the momentum balance equation becomes, in wall units,

$$(1 + \nu_p^+ R_{yy})S^+ + W^+ = 1 - \frac{y^+}{\mathcal{Re}}, \quad (6.2)$$

where $\nu_p^+ \equiv \nu_p/\nu_0$.

The energy balance equation remains as before,

$$W^+ S^+ \sim a^2 (1 + \nu_p^+ R_{yy}) \frac{K^+}{(y^+)^2} + b \frac{(K^+)^{3/2}}{y^+}. \quad (6.3)$$

As was explained above, equations (6.2) and (6.3) imply that the polymers change the properties of the flows by replacing the viscosity by

$$\nu_{\text{eff}} = 1 + \nu_p^+ R_{yy}. \quad (6.4)$$

In the fully developed turbulent flow with rod-like polymers, when \mathcal{Re} is very large, it was shown in (Benzi et al., 2005b) that R_{yy} depends on K^+ and S^+ :

$$R_{yy} = \frac{K^+}{(y^+ S^+)^2}. \quad (6.5)$$

It was argued in (Benzi et al., 2005b) that for large \mathcal{Re} , K^+ grows linearly with y^+ and thus the viscosity profile is linear.

Next consider low \mathcal{Re} flows. According to Eq. (6.4), the value of ν_{eff} depends on ν_p^+ and R_{yy} . The value of ν_p^+ is determined by the polymer properties such as the number of monomers, their concentration etc., and thus ν_p^+ should be considered as an external parameter in the equation. The value of R_{yy} , on the other hand, depends on the properties of the flow. In the case of laminar flow with a constant shear rate, i.e., $K^+ = W^+ = 0$ and $S^+ = \text{constant}$, it was shown theoretically in (Doi and Edwards, 1988) that:

$$R_{yy} = \frac{2^{1/3}}{\mathcal{De}^{2/3}}, \quad (6.6)$$

Thus, the effective viscosity is reduced if S is increased, and therefore the rod-like polymers solution is a shear-thinning liquid. Naturally, The value of \mathcal{De} changes with \mathcal{Re} . To clarify this dependence we consider the momentum equations Eq.(3.13) at $y = 0$ in the Newtonian case.

$$\nu_0 S = p' L. \quad (6.7)$$

Usually in experiments the system size and the working fluid remain the same. Therefore, ν_0 and L are constants

and so \mathcal{Re} depends on $p' L$ only. According to (1.1), \mathcal{Re}_τ grows as $\sqrt{p' L}$ and therefore

$$\mathcal{De} = \frac{\nu_0}{\gamma L^2} \mathcal{Re}^2 \quad (6.8)$$

by Eq.(6.7). Putting into Eq.(6.6), we have

$$\nu_{\text{eff}} = 1 + \nu_p^+ \frac{\lambda}{\mathcal{Re}_\tau^{4/3}}, \quad (6.9)$$

where $\lambda \equiv \nu_0/\gamma L^2$ is a constant.

In the case of intermediate \mathcal{Re} , we need an interpolation between Eqs. (6.5) and (6.6). To do this we note that when y^+ is small, the solution of Eqs. (2.6), (6.2) and (6.3) result in $W^+ = K^+ = 0$ in the viscous sub-layer. This implies that the flow cannot be highly turbulent in the viscous sub-layer. Thus, it is reasonable to employ Eq.(6.6) as long as y^+ is small. On the other hand, as the upper bound of y^+ is \mathcal{Re} , when y^+ is large, it automatically implies that \mathcal{Re} is large. The laminar contribution is therefore negligible as it varies inversely with \mathcal{Re} . The effective viscosity due to the polymer is dominated by the turbulent estimate, Eq. (6.5). To connect these two regions we simply use the pseudo-sum:

$$\begin{aligned} \nu_{\text{eff}} &= 1 + \nu_p^+ \left(\frac{\lambda}{\mathcal{Re}^{4/3}} + \frac{K^+}{(y^+ S^+)^2} \right) \\ &= g + \nu_p^+ \frac{K^+}{(y^+ S^+)^2}, \end{aligned} \quad (6.10)$$

where $g \equiv 1 + \nu_p^+ \lambda / \mathcal{Re}^{4/3}$. One can see that the limits for both high and low \mathcal{Re} are satisfied.

The form for (6.10) for ν_{eff} was incorporated into the balance equations which were analyzed and solved self-consistently in (Amarouchene et al., 2007) one of the most interesting results, which can be directly compared to the data in Fig. 5 refers to the drag reduction as a function of the concentration of the rod-like polymers, presented in Prandtl-Kármán coordinates. The results of the theoretical predictions are shown in Fig. 16, and the qualitative agreement with the experimental observations is obvious. Another interesting comparison with experimental findings is available due the work presented in (Amarouchene et al., 2007) where the percentage of drag enhancement and reduction were measure as a function of ν_p . The quantitative comparison needs a careful identification of the material parameters in the theory and the experiment, and this was described in detail in (Amarouchene et al., 2007). Fig. 17 shows the comparison of the percentage of drag reduction (enhancement) between the theoretical predictions and the experimental results. The two data sets shown pertain to $c_p = 250\text{wppm}$ and $c_p = 500\text{wppm}$. The agreement between theory and experiment is very satisfactory.

VII. DRAG REDUCTION BY BUBBLES

In order not to leave the reader with the impression that polymers are the only additives that can reduce the

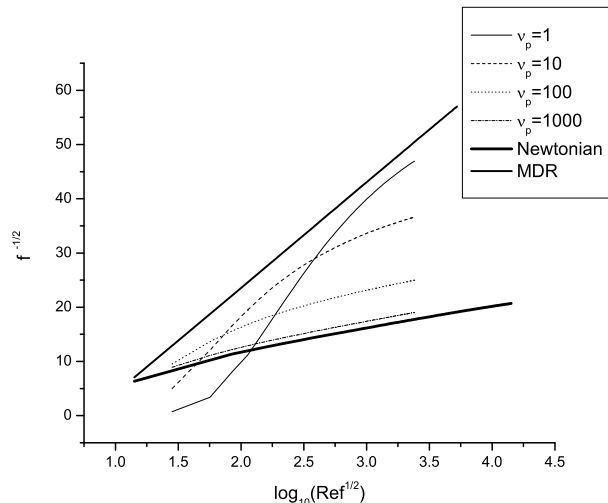


FIG. 16 $f^{-1/2}$ as the function of $\log_{10}(Re f^{1/2})$ with $\lambda = 1$ with various values of ν_p .

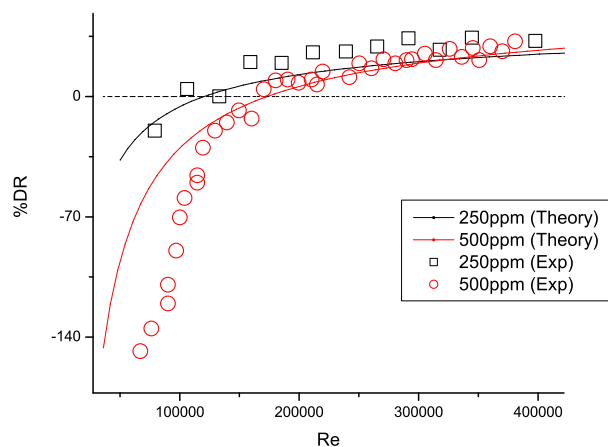


FIG. 17 Percentage drag reduction as a function of Re for two values of the concentration of the rod-like polymer. Symbols are results of experiments and solid lines—theory, cf. (Amarouchene et al., 2007)

drag, or that they provide the only technologically preferred method, we discuss briefly drag reduction by other additives like surfactants and bubbles (Gyr and Bewersdorff, 1995). Generally speaking, the understanding of drag reduction by these additives lags behind what had been achieved for polymers. The importance of drag reduction by bubbles cannot be however overestimated; for practical applications in the shipping industry the use of polymers is out of the question for economic and environmental reasons, but air bubbles are potentially very attractive (Kitagawa et al., 2005).

The theory of drag reduction by small concentrations

of minute bubbles is relatively straightforward, since under such conditions the bubbles only renormalize the density and the viscosity of the fluid, and a one-fluid model suffices to describe the dynamics (L'vov et al., 2005b). The fluid remains incompressible, and the equations of motion are basically the same as for a Newtonian fluid with renormalized properties. The amount of drag reduction under such conditions is however limited. But when the bubbles increase in size, the one-fluid model loses its validity since the bubbles become dynamical in the sense that they are no longer Lagrangian particles, their velocity is no longer the fluid velocity at their center, and they begin to fluctuate under the influence of local pressure variations. The fluctuations of the bubbles are of two types: 1) the bubbles are no longer spherical, distorting their shape according to the pressure variations, and 2) the bubbles can oscillate *radially* (keeping their spherical shape) due to the compressibility of the gas inside the bubble. The first effect was studied numerically using the “front tracking” algorithm of Kawamura and Kodama (2002); Lu et al. (2005). However, the results indicate either a drag enhancement, or a limited and transient drag reduction. This leads one to study the possibility of explaining bubbly drag reduction by bubble oscillations. Indeed, a theoretical model proposed by Legner (1984) successfully explained the bubbly drag reduction by relating turbulent viscosity in the bubbly flow to the bulk viscosity of the bubbles. While the bulk viscosity is important only when the bubbles are compressible, it is important and interesting to see how and why it affects the characteristics of the flow. Here we review how drag reduction is caused by bubbles when bubble oscillations are dominant. Finally we compare our finding with the results of Legner (1984), showing that a nonphysical aspect of that theory is removed, while a good agreement with experiment is retained.

A. Average equations for bubbly flows: the additional stress tensor

Dealing with bubbles we cannot put the fluid density to unity any longer and we must display it explicitly. Here a Newtonian fluid with density ρ is laden with bubbles of density ρ_B , and radius R which is much smaller than the outer scale of turbulence \mathcal{L} . The volume fraction of bubbles C is taken sufficiently small such that the direct interactions between bubbles can be neglected. In writing the governing equations for the bubbly flow we will assume that the length scales of interest are larger than the bubble radius. Later we will distinguish however between the case of microbubbles whose radius is smaller than the Kolmogorov scale η and bubbles whose radius is of the order of η or slightly larger. For length scales larger than the bubbles one writes (Biesheuvel and Wijngaarden, 1984; Sanghai and Didwania, 1993; Zhang and

Prosperetti, 1994):

$$\rho(1-C)\left[\frac{\partial \mathbf{U}}{\partial t} + \mathbf{U} \cdot \nabla \mathbf{U}\right] = -\nabla p + \nabla \cdot \boldsymbol{\sigma} + C \nabla \cdot \boldsymbol{\tau}. \quad (7.1)$$

$$\frac{\partial(1-C)}{\partial t} + \nabla \cdot (1-C)\mathbf{U} = 0. \quad (7.2)$$

In these equations, \mathbf{U} is the velocity of the carrier fluid, and

$$\sigma_{ij} \equiv \frac{\mu_0}{2} \left(\frac{\partial U_i}{\partial x_j} + \frac{\partial U_j}{\partial x_i} \right). \quad (7.3)$$

Here $\mu_0 = \rho\nu_0$. The effect of the bubbles appears in two ways, one through the normalization of the fluid density, $\rho \rightarrow \rho(1-C)$, and the second is via the extra stress tensor $\boldsymbol{\tau}$. Note that in the case of polymers we accounted only for the additional stress tensor since the actual volume fraction of polymers is minute, typically less than 10^{-3} . A typical value of the bubbles volume fraction is 0.05 or even more, and cannot be neglected.

The evaluation of the extra stress tensor $\boldsymbol{\tau}$ is tedious. There are a number of forces acting on bubbles, but following Lo et al. (2006) we neglect gravity and the lift force. In (Lo et al., 2006) it was found that the add-mass force due to bubble oscillations and the add-mass force due to bubble acceleration are of the same order of magnitude. The viscous forces were of course taken into account. The result is of the following form:

$$\boldsymbol{\tau} = \rho \left\{ \left[\frac{1}{4} (\mathbf{w} - \mathbf{U}) \cdot (\mathbf{w} - \mathbf{U}) - R\ddot{R} - \frac{5}{2} \dot{R}^2 \right] \mathbf{I} - \frac{1}{2} (\mathbf{w} - \mathbf{U})(\mathbf{w} - \mathbf{U}) + \frac{1}{2} \mu_0 \boldsymbol{\sigma} \right\}, \quad (7.4)$$

Here \mathbf{I} is the unit tensor, \mathbf{w} is the bubble velocity which differs from the carrier velocity \mathbf{U} . \dot{R} stands for the rate of change of the bubble radius R . The relative importance of the various terms in $\boldsymbol{\tau}$ depends on the values of Re and also on the so called Weber number, which is defined as

$$We \equiv \frac{\rho |\mathbf{w} - \mathbf{U}|^2 R}{\gamma}. \quad (7.5)$$

The Weber number is the ratio of the kinetic energy of the fluid associated with the bubble motion over the surface energy of the bubble itself due to surface tension γ . When $We \ll 1$ the bubbles can be considered as rigid spheres. If We is sufficiently large, the bubbles begin to deform and oscillate; this contributes a significant contribution to $\boldsymbol{\tau}$. In the following section we show that this can be crucial for drag reduction.

For very small bubbles (micro-bubbles) of very small density the last term in $\boldsymbol{\tau}$, i.e. $\mu_0 \boldsymbol{\sigma}$ which is the viscous contribution, is the only one that survives. When this is the case the bubble contribution to the stress tensor can be combined with $\boldsymbol{\sigma}$ in Eq. (7.1), resulting in the effective viscosity given by

$$\mu_{\text{eff}} = \left(1 + \frac{5}{2}C\right)\mu. \quad (7.6)$$

The study of drag reduction under this renormalization of the viscosity and the density was presented in (L'vov et al., 2005b) with the result that drag reduction can be obtained by putting the bubbles out of the viscous sub-layer and not too far from the wall. The amount of drag reduction is however rather limited in such circumstances.

B. Balance equations in the turbulent boundary layer

At this point we apply the formalism detailed above to the question of drag reduction by bubbles in a stationary turbulent boundary layer with plain geometry. This can be a pressure driven turbulent channel flow or a plain Couette flow, which is close to the circular Couette flow realized in (van den Berg et al., 2005). As before, we take the smallest geometric scale to be $2L$, the unit vector in the streamwise and spanwise directions be \hat{x} and \hat{z} respectively, and the distance to the nearest wall be $y \ll L$. The variables that enter the analysis are modified by the density, except for the mean shear, which remains as in Eq. (2.2). The turbulent kinetic energy density is modified to read

$$\mathcal{K} \equiv \frac{1}{2} \rho(1-C) \langle |\mathbf{u}|^2 \rangle, \quad (7.7)$$

and the Reynolds stress

$$\mathcal{W} \equiv -\rho(1-C) \langle u_x u_y \rangle. \quad (7.8)$$

1. Momentum balance

From Eq. (7.1) we derive the exact equation for the momentum balance by averaging and integrating in the usual way, and find for $y \ll L$:

$$\rho P = \mu_0 S + \mathcal{W} + C \langle \tau_{xy} \rangle. \quad (7.9)$$

Here P is the momentum flux toward the wall.

For $C = 0$ Eq. (7.9) is the usual Eq. (3.13) satisfied by Newtonian fluids. To expose the consequences of the bubbles we notice that the diagonal part of the bubble stress tensor $\boldsymbol{\tau}$ [the first line in the RHS of Eq. (7.4)] does not contribute to Eq. (7.9). The xy component of the off-diagonal part of $\boldsymbol{\tau}$ is given by the 2nd line in Eq. (7.4). Define the dimensionless ratio

$$\zeta \equiv \frac{\langle (w_x - U_x)(w_y - U_y) \rangle}{2 \langle u_x u_y \rangle}. \quad (7.10)$$

For later purposes it is important to assess the size and sign of ζ . This object was analyzed in (Lo et al., 2006), and it was shown that for small values of Re , ζ is small. On the other hand, for large Re the fluctuating part of \mathbf{w} is closely related to the fluctuating part of \mathbf{u} . The relation is

$$\mathbf{w} - \mathbf{U} \approx 2\mathbf{u}. \quad (7.11)$$

This implies that $\zeta \approx 2$ and is positive definite, as we indeed assume below. With this definition we can simplify the appearance of Eq. (7.9):

$$\rho P = \mu_{\text{eff}} S + \frac{1 + C(\zeta - 1)}{1 - C} \mathcal{W}, \quad (7.12)$$

with μ_{eff} defined by (7.6).

2. Energy balance

Next, we consider the balance of turbulent energy in the log-layer. In this region, the production and dissipation of turbulent kinetic energy is almost balanced. The production can be calculated exactly, $\mathcal{W}S$. The dissipation of the turbulent energy is modeled by the energy flux which is the kinetic energy $\mathcal{K}(y)$ divided by the typical eddy turn over time at a distance y from the wall, which is $\sqrt{\rho(1-C)y/b\sqrt{\mathcal{K}}}$ where b is a dimensionless number of the order of unity. Thus the flux is written as $b\mathcal{K}^{3/2}/y\sqrt{\rho(1-C)}$. The extra dissipation due to the bubble is $C\langle\tau_{ij}s_{ij}\rangle$ where $s_{ij} \equiv \partial u_i/\partial x_j$. In summary, the turbulent energy balance equation is then written as:

$$\frac{b\mathcal{K}^{3/2}}{\sqrt{\rho(1-C)}y} + C\langle\tau_{ij}s_{ij}\rangle = \mathcal{W}S. \quad (7.13)$$

As usual, the energy and momentum balance equations do not close the problem, and we need an additional relation between the objects of the theory, and we define c_B in a manner following Eq. (2.6):

$$\mathcal{W} \equiv c_B^2 \mathcal{K}. \quad (7.14)$$

Clearly, $\lim_{C \rightarrow 0} c_B = c_N$ and for small C (noninteracting bubbles) $c_B^2 - c_N^2 \propto C$. Having in mind that in numerical simulations of the incompressible bubbly flow, it was reported (Bellakhel et. al., 2004; Lance et. al., 1991) that c_B is slightly smaller than its Newtonian counterpart we can write

$$c_B^2 = c_N^2(1 - \tilde{\beta}C), \quad (7.15)$$

with positive coefficient $\tilde{\beta}$ of the order of unity. We are not aware of direct measurements of this form in bubbly flows, but it appears natural to assume that the parameter $\tilde{\beta}$ is y -independent in the turbulent log-law region.

C. Drag reduction in bubbly flows

In this section we argue that bubble oscillations are crucial in enhancing the effect of drag reduction. This conclusion is in line with the experimental observation of (van den Berg et al., 2005) where bubbles and glass spheres were used under similar experimental conditions. Evidently, bubble deformations can lead to the compressibility of the bubbly mixture. This is in agreement with

the simulation of (Ferrante and Elgobashi, 2004) where a strong correlation between compressibility and drag reduction were found.

To make the point clear we start with the analysis of the energy balance equation (7.13). The additional stress tensor τ_{ij} Eq. (7.4) has a diagonal and an off diagonal part. The off-diagonal part has a viscous part that is negligible for high Re. The other term can be evaluated using the estimate (7.11), leading to a contribution to $\langle\tau_{ij}s_{ij}\rangle$ written as

$$\left\langle \frac{1}{2}(\mathbf{w} - \mathbf{U})(\mathbf{w} - \mathbf{U}) : \nabla \mathbf{u} \right\rangle \approx 2\langle \mathbf{u}\mathbf{u} : \nabla \mathbf{u} \rangle. \quad (7.16)$$

The expression on the RHS is nothing but the spatial turbulent energy flux which is known to be very small in the log-layer compared to the production term on the RHS of Eq. (7.13). We will therefore neglect the off-diagonal part of the stress tensor in the energy equation. The analysis of the diagonal part of the stress depends on the issue of bubble oscillations and we therefore discuss separately oscillating bubbles and rigid spheres.

1. Drag reduction with rigid spheres

Consider first situations in which $\dot{R} = 0$. This is the case for bubbles at small We, or when the bubbles are replaced by some particles which are less dense than the carrier fluid (van den Berg et al., 2005). When the volume of the bubbles is fixed, the incompressibility condition for the Newtonian fluid is unchanged, and $s_{ii} = 0$. The diagonal part of τ , Eq. (7.4), due to the incompressibility condition $s_{ii} = 0$, has no contribution to $\langle\tau_{ij}s_{ij}\rangle$. Due to the discussion after Eq. (7.16) the term due to the extra stress tensor can be neglected and the energy balance equation is then unchanged compared to the Newtonian fluid. Note that the momentum balance equation is nevertheless affected by the bubbles. Putting (7.14) into (7.13), we have after simple algebra

$$\mathcal{W} = \rho(1 - C) \frac{S^2 y^2 c_B^6}{b^2}. \quad (7.17)$$

To assess the amount of drag reduction we will consider an experiment (Kitagawa et al., 2005) in which the velocity profile (and thus S) is maintained fixed. Drag reduction is then measured by the reduction in the momentum flux P . Substituting Eq. (7.17) into Eq. (7.12) in which one can neglect $\mu_{\text{eff}}S$, and replacing $S(y)y = 1/\kappa_K$ we find

$$P = \frac{\rho(1 - C + \zeta C)c_B^6}{\kappa_K^2 b^2}. \quad (7.18)$$

If there are no bubbles ($C = 0$), the Newtonian momentum flux P_N reads

$$P_N = \frac{\rho c_N^6}{\kappa_K^2 b^2}. \quad (7.19)$$

The percentage of drag reduction can be defined as

$$\begin{aligned} \%DR &= \frac{P_N - P}{P_N} = 1 - \frac{(1 - C + \zeta C)c_B^6}{c_N^6} \\ &\approx (1 - \zeta + 3\tilde{\beta})C. \end{aligned} \quad (7.20)$$

At small Re , $\zeta = 0$ and the amount of drag reduction increases linearly with C . If Re is very large we expect $\zeta \approx 2$, and then the drag is *enhanced*. This result is in pleasing agreement with the experimental data in (van den Berg et al., 2005). Indeed, the addition of glass beads with density less than water caused drag *reduction* when Re is small, whereas at $Re \sim (10^6)$, the drag was slightly *enhanced*.

2. Drag reduction with flexible bubbles

If the value of We is sufficiently large such that $\dot{R} \neq 0$, the velocity field is no longer divergenceless. Also, to evaluate the extra stress tensor one needs the explicit dynamical equation for the bubble radius. This equation was provided by Zhang and Prosperetti (1994), and was analyzed carefully in (Lo et al., 2006). Using the results of the analysis in Eq. (7.4) one can simplify the extra stress tensor (for calculating the correlation $\langle \tau_{ij} s_{ij} \rangle$) to the form

$$\boldsymbol{\tau} \approx \rho \left[\frac{4}{3} \mu \nabla \cdot \mathbf{u} \mathbf{I} + \frac{1}{2} (\mathbf{w} - \mathbf{U})(\mathbf{w} - \mathbf{U}) \right] \quad (7.21)$$

The extra turbulent dissipation due to the bubble is $\langle \tau_{ij} s_{ij} \rangle$. In light of the smallness of the term in Eq. (7.16) we find

$$\langle \tau_{ij} s_{ij} \rangle = \frac{4}{3} \mu s_{ii}^2. \quad (7.22)$$

The term $\frac{4}{3} \mu s_{ii}^2$ is of the same form as the usual dissipation term $\mu s_{ij} s_{ij}$ and therefore we write this as:

$$\left\langle \frac{4}{3} \mu s_{ii}^2 \right\rangle = A \frac{\rho |\mathbf{u}|^{3/2}}{y} = A \frac{\mathcal{K}^{3/2}}{\sqrt{\rho} (1 - C)^{3/2} y} \quad (7.23)$$

where A is an empirical constant. Finally, the energy equation becomes

$$\frac{b(1 - C) + AC}{\rho \sqrt{1 - C}} \frac{\mathcal{K}^{3/2}}{y} = \mathcal{W}S \quad (7.24)$$

As we derived Eq. (7.19), we again specialize the situation to an experiment in which S is constant, and compute the momentum flux

$$P = \frac{(1 - C)^2 (1 - C + \zeta C)}{(1 - C + \frac{A}{b} C)^2} \frac{c_B^6}{\kappa_K^2 b^2}. \quad (7.25)$$

The degree of drag reduction is then

$$\%DR = 1 - \frac{(1 - C)^2 (1 - C + \zeta C)}{(1 - C + \frac{A}{b} C)^2} \left(\frac{c_B}{c_N} \right)^6. \quad (7.26)$$

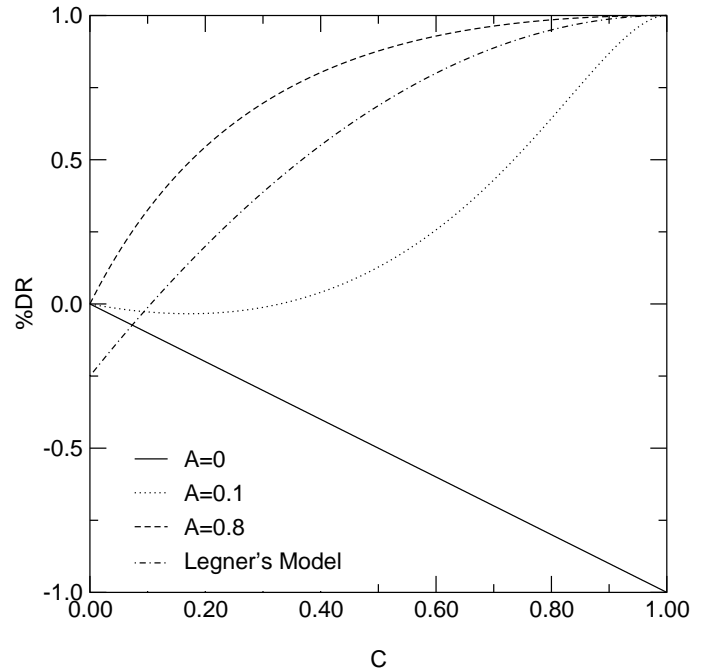


FIG. 18 Predicted values of drag reduction with $\alpha = 2$ and different values of A . In a dashed line we reproduce the predictions of Legner's theory which suffer from an unphysical drag enhancement at $C = 0$. For $A = 0$ (rigid spheres) we find only increasing drag enhancement as a function of C . For small values of A we have first a slight drag enhancement, and then modest drag reduction. For large values of A , associated with strong bubble oscillations, we find significant values of drag reduction.

Note that A is an unknown parameter that should depend on We , and so its value is different in different experiments. The percentage of drag reduction for various values of A are shown in Fig. 18 where we chose $\alpha = 2$ and for simplicity we estimate $c_B = c_N$. One sees that for $\alpha = 2$ and $A = 0$ (where the latter is associated with rigid bubbles), we only find drag enhancement. For small value of A , or small amplitudes of oscillations, small concentrations of bubbles lead (for $\alpha = 2$) to drag enhancement, but upon increasing the concentration we find modest drag reduction. Larger values of A lead to considerably large degrees of drag reduction. For $A = 0.15$, the result agrees reasonably with Legner's theory which predicts $\%DR \approx 1 - 5(1 - C)^2/4$ (Legner, 1984). Note that according to Legner, there should be considerable drag enhancement when $C = 0$. This is of course a nonsensical result that is absent in our theory. For $A = 0.8$, $\%DR \approx 4C$ for small C . This is the best fit to the experimental results which are reported in (Kitagawa et al., 2005).

VIII. SUMMARY AND DISCUSSION

We offered a review of drag reduction by polymers and bubbles. Quite generally, we have shown that drag reduc-

tion can be understood in great detail by using only a few equations that govern the budgets of energy and momentum. Both polymers and bubbles open up an additional channel for dissipation, and thus pose a fundamental riddle: why do they reduce the drag. The answer in all cases is fundamentally the same: the same agents reduce the momentum flux from the bulk to the wall, and this is the main effect leading to drag reduction. The reduction in the momentum flux overwhelms the increase dissipation. We stressed above, and we re-iterate here, that this mechanism depends on the existence of a wall which breaks the translational symmetry. Drag reduction must be discussed in the context of wall-bounded flows to make full sense. Of course, additives may influence also the spectrum of turbulent fluctuations in homogeneous and isotropic turbulence, but this is another story, quite independent of drag reduction.

One should make a great distinction between the two cases. The phenomenon of drag reduction by polymers exhibits interesting universal features which are shared even by flexible and rod-like polymers. These features are the most prominent experimental results that required theoretical understanding. We have shown that the MDR has a special significance in being an edge solution of turbulent flows. Trying to increase the reduction of the drag behind what is afforded by the MDR would re-laminarize the flow. This may be the central theoretical insight that is offered in this review, providing a simple and intuitive meaning to the nature of the MDR. This explains why flexible and rod-like polymers have the same MDR, even though they approach the MDR in distinctly different ways.

Once the theory was put forth to explain the universal aspects of drag reduction by polymers, it became also clear that it can easily explain, in considerable quantitative detail, also the non-universal aspects, including cross-overs due to small concentrations of polymers, low values of $\mathcal{R}e$, and small number of monomers in the polymer chains. We trust that this detailed understanding can help in designing and optimizing the use of polymers in practical applications of drag reduction.

On the other hand, the case of bubbles exhibits much less universality, since the placement of the bubbles with respect to the wall and their actual density profile have crucial consequences regarding their efficacy as drag reducers. The main conclusion of our study is that bubble oscillations can contribute decisively to drag reduction in turbulent flows. In agreement with the experimental findings of (van den Berg et al., 2005), we find that rigid bubbles tend to drag enhance, and the introduction of oscillations whose amplitude is measured by the parameter A (Fig. 18) increases the efficacy of drag reduction. The main drawback of the present study is that the bubble concentration was taken uniform in the flow. In reality a profile of bubble concentration may lead to even stronger drag reduction if placed correctly with respect to the wall. A consistent study of this possibility calls for the consideration of buoyancy and the self-consistent so-

lution of the bubble concentration profile. Such an effort is beyond the scope of this review and must await future progress.

Acknowledgments

We thank our collaborators Emily S.C. Ching, Elisabetta DeAngelis, Ting-Shek Lo, Anna Pomyalov and Vasily Tiberkevich without whom the research reviewed in this paper could not be accomplished. Albert Libchaber and Ting-Shek Lo have read the manuscript and made a number of valuable comments and suggestions. This work has been supported in part by the US-Israel Binational Science Foundation, by the European Commission under a TMR grant, and by the Minerva Foundation, Munich, Germany.

*

APPENDIX A: The Hidden Symmetry of the Balance Equations

Consider the following identity:

$$\begin{aligned} \nu^+(y^+) &= 1 + \alpha(y^+ - \delta^+) \\ &= [1 + \alpha(y^+ - \delta) + \alpha(\delta - \delta^+)] \\ &= g(\delta) \left[1 + \frac{\alpha}{g(\delta)}(y^+ - \delta) \right], \end{aligned} \quad (\text{A1})$$

where

$$g(\delta) \equiv 1 + \alpha(\delta - \delta^+), \quad \delta \geq \delta^+. \quad (\text{A2})$$

Next introduce newly renormalized units using the effective viscosity $g(\delta)$, i.e.

$$y^\ddagger \equiv \frac{y^+}{g(\delta)}, \quad \delta^\ddagger \equiv \frac{\delta}{g(\delta)}, \quad S^\ddagger \equiv S^+ g(\delta), \quad W^\ddagger \equiv W^+. \quad (\text{A3})$$

In terms of these variables the balance equations are rewritten as

$$[1 + \alpha(y^\ddagger - \delta^\ddagger)] S^\ddagger + W^\ddagger = 1, \quad (\text{A4})$$

$$[1 + \alpha(y^\ddagger - \delta^\ddagger)] \frac{\Delta^2(\alpha)}{y^{\ddagger 2}} + \frac{\sqrt{W^\ddagger}}{\kappa_\kappa y^\ddagger} = S^\ddagger. \quad (\text{A5})$$

These equations are isomorphic to (3.19) and (3.20) with δ^+ replaced by δ^\ddagger . The ansatz (3.21) is then replaced by $\Delta(\alpha) = \delta^+ g(\delta)^{-1} f(\alpha \delta^\ddagger)$. This form is dictated by the following considerations: (i) $\Delta(\alpha) \rightarrow \delta^+$ when $\alpha \rightarrow 0$, (ii) all lengths scales in the re-scaled units are divided by $g(\delta)$, and thus the pre-factor in front of f becomes $\delta^+ / g(\delta)$, and (iii) $\alpha \delta^+$ in Eq. (3.18) is now replaced in Eq. (A5) by $\alpha \delta^\ddagger$, leading to the new argument of f . Since the function $\Delta(\alpha)$ cannot change due to the change of

variables, the function $\Delta(\alpha)$ should be identical to that given by Eq. (3.21):

$$\delta^+ f(\alpha\delta^+) = \frac{\delta^+}{g(\delta)} f(\alpha\delta^\ddagger). \quad (\text{A6})$$

Using the explicit form of $g(\delta)$ Eq. (A2), and choosing (formally first) $\delta = \delta^\ddagger = 0$ we find that $f(\xi) = 1/(1 - \xi)$. It is easy to verify that this is indeed the solution of the above equation for any value of δ^\ddagger , and therefore the unique form of Eq. (3.22).

References

- Y. Amarouchene, D. Bonn, H.Kellay, T.S. Lo, V. S. L'vov and I Procaccia, 2007, "Reynolds number dependence of drag reduction by rod-like polymers", submitted to Phys. Fluids, Also: nlin.CD/0607006
- G. Bellakhel, J. Chahed and L. Masbernat, 2004, J. Turbul. **5**, 036.
- R. Benzi, E. Ching, N. Horesh and I. Procaccia, 2004, Phys. Rev. Lett. **93**, 078302.
- R. Benzi, V. S. L'vov, I. Procaccia and V. Tiberkevich, 2004 Europhys. Lett., **68**, 825.
- R. Benzi, E. deAngelis, V.S. L'vov and I. Procaccia, 2005, Phys. Rev. Lett., **95** 194502.
- R. Benzi, E. S.C. Ching, T. S. Lo, V. S. L'vov, and I. Procaccia, 2005, Phys. Rev. E, **72**, 016305.
- R. Benzi, E. de Angelis, V. S. L'vov, I. Procaccia and V. Tiberkevich, 2006, J. Fluid Mech. **551**, 185.
- T. H. van den Berg, S. Luther, D. P. Lathrop and D. Lohse, 2005, Phys. Rev. Lett., **94** 044501.
- A.N. Beris and B.J. Edwards, 1994, *Thermodynamics of Flowing Systems with Internal Microstructure* (Oxford University Press).
- A. Biesheuvel and L. wan Wijngaarden, 1984, J. Fluid Mech. , **148** 301.
- R.B. Bird, C.F. Curtiss, R.C. Armstrong, O. Hassager, 1987, *Dynamics of Polymeric Fluids* (Wiley, NY).
- D. Bonn, Y. Amarouchène, C. Wagner, S. Douady and O. Cadot, 2005, J. Phys.: Condens. Matter, **17**, S1195.
- H. Brenner, 1974, Int. J. Multiphase Flow **1**, 195.
- E. S.C. Ching, T. S. Lo, I. Procaccia, 2006, Phys. Rev. E, **74**, 026301.
- H.J. Choi, S.T. Lim, P-Y Lai and C.K. Chan, 2002, Phys. Rev. Lett, **89** 088302-1.
- E. De Angelis, C. M. Casciola, V. S. L'vov, R.Piva and I. Procaccia, 2003 Phys. Rev. E., **67** 056312 (2003).
- E. De Angelis, C. Casciola, V. S. L'vov, A. Pomyalov, I. Procaccia and V. Tiberkevich, 2004. Phys. Rev. E, **70**, 055301.
- E. De Angelis, C. M. Casciola, R. Benzi and R.Piva, 2005, J. Fluid Mech. **531**, 1.
- M. Doi and S. F. Edwards, 1988, *The Theory or Polymer Dynamics*, Oxford University Press.
- P.-G. de-Gennes, 1979, *Scaling Concepts in Polymer Physics* Cornell University University.
- P.-G. de-Gennes, 1990, *Introduction to Polymer Dynamcis* Cambrdige University Press.
- A. Gyr and H. W. Bewersdorff, 1995, *Drag Reduction of Turbulent Flows by Additives* Kluwe, London.
- C.D. Dimitropoulos, S. Sureshkumar and A.N. Beris, 1998, J. Non-Newtonian Fluid Mech. **79**, 433 (1998).
- C.D. Dimitropoulos, Y. Dubief, E.S.G. Shawfeh, P. Moin and S.K. Lele, 2005, Phys. Fluids, **17**, 011705-1.
- M. P. Escudier, P. Presti and S. Smith, 1999, J. Non-Newtonian Fluid Mech. **81**, 197.
- A. Ferrante and S. Elghobashi, 2004, J. Fluid Mech. , **503** 345.
- P.J. Flory, 1953 *Principles of Polymer Chemistry*, (Cornell University)
- E. Hinch and L. Leal, 1975, J. Fluid Mech. **71**, 481.
- E. Hinch and L. Leal, 1976, J. Fluid Mech. **76**, 187.
- J.W. Hoyt, 1972, Trans. ASME:J. Basic Engng **94**, 258.
- T. Kawamura and Y. Kodama, 2002, Int. J. Heat and Fluid Flow **23**, 627.
- A. Kitagawa, K. Hishida and Y. Kodama, 2005 Experiment in Fluids , **38** 466.
- M.T. Landhal, 1973, in *Proc. 13th Intl. Congr. Theor. Appl. Mech., Moscow* (ed. E. Becker and G.K. Mikhailov), 179. Springer.
- H. Lamb, 1879, *Hydrodynamics*, Dover reprint 1945.
- M. Lance, J.L. Marie and J. Bataille, 1191, J. Fluid Eng. **113**, 295.
- H. H. Legner, 1984, Phys. Fluids , **27** 2788.
- J.L. Lumley, 1969, Ann. Rev. Fluid Mech. **1**, 367.
- T.S. Lo, V. S. L'vov, A. Pomyalov and I. Procaccia, 2005, Europhys. Lett., **72**, 943.
- T.S. Lo, Victor S. L'vov and I. Procaccia, 2006, Phys. Rev. E., **73**, 036308.
- V. S. L'vov, A. Pomyalov, I. Procaccia and V. Tiberkevich, 2004, Phys. Rev. Lett., **92** 244503.
- V. S. L'vov, A. Pomyalov, I. Procaccia and V. Tiberkevich, 2005, Phys. Rev. E **71**, 016305.
- V. S. L'vov, A. Pomyalov, I. Procaccia and V. Tiberkevich, 2005, Phys. Rev. Lett., **94** 174502.
- V. S. L'vov, A. Pomyalov and V. Tiberkevich, 2005, Environmental Fluid Mechanics, **5**, 373.
- J. Lu, A. Fernandez, and G. Tryggvason, 2005, Phys. Fluids **17**, 095102.
- M. Manhart, 2003, J. NON-Newtonian Fluid Mech. **112**, 269.
- W. McComb, 1990, *The fluid of Physics Turbulence*, Clarendon.
- A. S. Monin and A. M. Yaglom, 1979, *Statistical Fluid Mechanics* (MIT, 1979, vol. 1 chapter 3).
- S. B. Pope, 2000, *Turbulent Flows*, Cambridge University Press.
- P.K. Ptasinski, F.T.M. Nieuwstadt, B.H.A.A. van den Brule and M.A. Hulsen, 2001, Flow Turbul. Combust, **66**, 159.
- A. Rollin and F.A. Seyer, 1972, Can. J. Chem. Eng, **50**, 714.
- M.J. Rudd, 1969, Nature, **224**, 587.
- A. S. Sangani and A. K. Didwania, 1993, J. Fluid Mech. , **248** 27.
- S. Sibila and A. Baron, 2002, Phys. Fluids **14**, 1123.
- K.R. Sreenivasan and C.M. White, 2000, J. Fluid Mech., **409** 149.
- B.A. Toms, 1949 in *Proc. Intl. Rheological Congress Holland, 1948, p. 135*.
- J. M. J. den Toonder, F. T. M. Nieuwstadt and G. D. C. KuiKen , 1995 Appl Sci Res, **54**, 95.
- P.S. Virk, 1975, AIChE J. **21**, 625.
- P. S. Virk, D. L. Waggar and E. Koury, 1996, ASME FED- **237**, 261.
- P.S. Virk, D.C. Sherma and D.L. Waggar, 1997, AIChE J., **43**, 3257.
- C. Wagner, Y. Amarouchène, P. Doyle and D. Bonn, 2003, Europhys. Lett. **64**, 823.

- M.D. Warholic, H. Massah and T.J. Hanratty, 1999, *Exp. Fluids* **27**, 461
- B. Yu, Y. Kawaguchi, S. Takagi and Y. Matsumoto, 2001, *7th Symposium on Smart Control of Turbulence* University of Tokyo.
- M.V. Zagarola and A.J. Smits, 1997, *Phys. Rev. Lett.* **78**, 239.
- D. Z. Zhang and A. Prosperetti, 1994, *Phys. Fluids*, **6**, 2956.